Journal of South American Earth Sciences 168 (2025) 105826

Contents lists available at ScienceDirect

Journal of South American Earth Sciences

journal homepage: www.elsevier.com/locate/jsames

A convergence model for the SW Gondwana margin during the late Paleozoic based on the structural analysis of accretionary complexes in northern and south-central Chile

Juan Díaz-Alvarado [a,*], Carlos Fernández [b], Andrés Folguera [c], Christian Creixell [d], Verónica Oliveros [e], Juan Carlos Moral [e]

[a] Departamento de Biología y Geología, Física y Química Inorgánica, ESCET, Universidad Rey Juan Carlos, Av. del Alcalde de Móstoles, 28933, Móstoles, Spain
[b] Departamento de Geodinámica, Estratigrafía y Paleontología, Facultad de Ciencias Geológicas, Universidad Complutense de Madrid, 28040, Madrid, Spain
[c] Departamento de Ciencias Geológicas, Facultad de Ciencias Exactas y Naturales, Instituto de Estudios Andinos (Don Pablo Groeber), Universidad de Buenos Aires - CONICET, Buenos Aires, Argentina
[d] Servicio Nacional de Geología y Minería, Avenida Santa María 0104, 7520405, Providencia, Santiago, Chile
[e] Departamento Ciencias de la Tierra, Universidad de Concepción, Casilla 160-C, Concepción, Chile

ARTICLE INFO

Keywords:
Accretionary complexes
Tectonic mélange
Structural analysis
Convergence style
Gondwanan cycle

ABSTRACT

This study presents a comprehensive analysis of the convergence style in the accretionary complexes along the Chilean coast, focusing on the structural study of the Maule River section (35° S), to shed light on the complexity of the subductive southwestern Gondwana margin during the late Paleozoic. The Maule River section, part of the Coastal Accretionary Complex of Central Chile, provides insights into the structural configuration of the basal and frontal accretionary wedge, and is compared in this work with the Chañaral mélange, more than 1000 km to the north. The structural analysis reveals significant differences in the convergence parameters (subduction zone boundary azimuth, convergence direction, flow trajectories). The aim of this study is to assess the influence of convergence style on the differences in lithological, metamorphic, and structural characteristics between these two widely separated fragments of the Carboniferous accretionary complex.

The Maule River section is characterized by two well-differentiated sectors: the Eastern Series, comprising low-grade phyllites and quartzites, and the Western Series, consisting of albite-bearing pelitic schists, greenschists and amphibolites, recording medium-high pressure conditions and temperatures below 500 °C. To the east, the Carboniferous magmatic arc and its basement are tectonically juxtaposed to the metasedimentary wedge.

The Eastern Series exhibits structures with opposed vergences: eastward in the eastern area and west-northwestward in the central and western areas. In contrast, the Western Series shows different structural patterns, including isoclinal folds and abundant S-C structures. The main schistosity presents E-W to N-S directions dipping moderately to the south and east respectively. The mineral and stretching lineation trends mostly E-W to NW-SE with low plunges towards the east and southeast, indicating top-to-the-WNW displacement.

A 3D kinematic model applied to the structural data collected in the Maule river section results in a triclinic to monoclinic transpressive shear zone (subduction channel and its influence zone), with a constrictional coaxial component ($K = 5$) and with the simple shear direction acting parallel to the dip of the subduction zone boundary. The particle flow trajectories (extrusion direction) fluctuated ±60° around the convergence direction of N123E ±24°, orthogonal to the margin azimuth. In the Chañaral area, both the convergence direction (N50-60E) and the extrusion trajectories predicted for the materials in the shear zone, with a low pitch on the boundary of the deformation zone, contrast with the results obtained in the Coastal Accretionary Complex of Central Chile. The differences in the late Paleozoic margin configuration may partially explain the absence of high-pressure rocks in the north (Chañaral area), although other post-accretionary processes such as tectonic erosion and block rotations may accentuate these differences.

Besides, the study concludes that the Maule River section's double vergence can be explained by the pro-wedge and retro-wedge structure established in wide accretionary prisms. The results highlight the

This article is part of a special issue entitled: Dedicated to V Ramos published in Journal of South American Earth Sciences.

* Corresponding author.
E-mail address: juan.diaz@urjc.es (J. Díaz-Alvarado).

https://doi.org/10.1016/j.jsames.2025.105826
Received 8 April 2025; Received in revised form 16 September 2025; Accepted 7 October 2025
Available online 8 October 2025

importance of performing 3D kinematic studies in tectonic mélanges to obtain a complete tectonic picture of the activity and characteristics of the entire subduction system during the late Paleozoic.

1. Introduction

The complexity of subductive continental margins, where the interaction between different lithologies from both plates occurs under the kinematic regime imposed by convergence dynamics, is recorded in accretionary complexes (e.g., Cloos and Shreve, 1988a, b; Condie, 2007). From the deepest regions of the basal domains—characterized by ductile deformation of high-grade metamorphic rocks of both continental and oceanic origin—to the frontal parts of the prism, where brittle-ductile deformation zones accommodate convergence-related shortening, the lithological, structural, metamorphic, and even geochronological features show marked variations both along-dip and along-strike of the margin (e.g., Díaz-Alvarado et al., 2019).

From a structural and kinematic perspective, the basal zones of the prism and the subduction channel can be considered as a major shear zone, representing the interaction area between tectonic plates and their influence zone (e.g., Kimura et al., 2007; Escuder-Viruete and Baumgartner, 2014). Mélanges and broken formations, characterized by block-in-matrix units (Cloos, 1982; Shreve and Cloos, 1986; Festa et al., 2010, 2012; Raymond, 1984), or the stacking of oceanic and metasedimentary tectonic slices (e.g., Glodny et al., 2005; Hyppolito et al., 2015; Muñoz-Montecinos et al., 2020), are typical highly deformed units in these settings. Key structures in these formations include mylonitic shear zones, pinch-and-swell structures, boudins, isoclinal and sheath folds, and S-C-C' structures, among others (Festa et al., 2012; Taira et al., 1992; Bettelli and Vannucchi, 2003; Ohsumi and Ogawa, 2008; Grigull et al., 2012). The vergences of these structures align with the relative motions of convergent tectonic plates (Shi et al., 2013; Escuder-Viruete and Baumgartner, 2014; Kato and Godoy, 2015; Fuentes et al., 2016, 2019).

Oblique convergence at subductive plate boundaries typically results in three-dimensional deformation patterns (Philippon and Corti, 2016; Díaz Azpiroz et al., 2016; 2019). However, most studies have focused on two-dimensional models orthogonal to the trench, which do not fully capture the complexity of mélange processes (Cloos, 1982; Niwa, 2006; Plunder et al., 2018). Understanding the three-dimensional kinematics of these complex deformation zones, including kinematic modeling of transpression and transtension, is essential for comprehending the evolution of ancient subductive margins (e.g., Fuentes et al., 2019).

Accretionary complexes represent only a portion of the geological record left by the Gondwanan cycle in Chilean territory and on the Argentine side of the Andes. Carboniferous and early Permian formations adjacent to the accretionary complexes are interpreted as forearc volcanosedimentary deposits (e.g., Llano del Chocolate Beds or Huentelauquén Formation) (e.g., Creixell et al., 2016; Charrier et al., 2024). There is an extensive registry of deposits on the Argentine side corresponding to the Gondwanan backarc (e.g., Limarino et al., 2023). Additionally, the Carboniferous and Lower Permian magmatic arc is studied in several segments of the central and northern Chilean Andes, although in the south-central region (33–38° S), and it can be found in the coastal range, between 0 and 30 km *from* the accretionary complexes (Creixell et al., 2025 and references therein). Parts of these late Carboniferous to early Permian rocks were obliterated during more than 200 million years of the Andean cycle. Nevertheless, the evolution of the margin during this period, which connects the Paleozoic accretionary stage with the stable (in terms of crustal growth) Andean cycle, can only be understood by correlating the processes occurring in all settings along the continental margin.

This study aims to provide new insights into the role of convergence style in shaping the architecture of Carboniferous accretionary complexes along the southwestern Gondwana margin. By comparing the structural configuration of two widely separated segments—the Maule River section and the Chañaral mélange—this work highlights how variations in convergence parameters (such as subduction zone boundary azimuth, convergence direction, and flow trajectories) may have controlled the contrasting lithological, metamorphic, and structural features observed in each area. These findings emphasize the need to re-evaluate the tectonic significance of Carboniferous metamorphic outcrops along the Chilean coast using integrated structural approaches and 3D kinematic modeling, moving beyond traditional 2D tectono-metamorphic interpretations.

2. Tectonic scenario/Geodynamic background

The tectonic evolution preceding the so-called Gondwanan cycle is one of the least understood aspects of the Paleozoic evolution of southwestern Gondwana. Following the dismantling of the Famatinian orogen (e.g., Weinberg et al., 2018; Otamendi et al., 2020), large masses of post-orogenic granite were emplaced in the Eastern Sierras Pampeanas (Fig. 1a) (Dahlquist et al., 2021). In contrast, calc-alkaline magmatism was minimal and localized. Some authors have used these bodies to propose the continuity of subduction to the west of the accreted terranes (e.g., Dahlquist et al., 2018, 2021). However, the most accepted hypothesis is the prevalence of a passive margin between 27° and 34°S once the continental masses of Cuyania and Chilenia were accreted (e.g., Bahlburg et al., 2009; Hervé et al., 2013, 2016). The continuity of this passive margin to the north and south is debated: north of 27°S, although a passive margin is traditionally suggested, some authors have proposed a nearly amagmatic subduction based on the presence of a few intermediate arc lavas (Bahlburg, 2021). To the south, the most accepted hypothesis is the existence of intra-oceanic subduction, forming an island arc called Chaitenia, which eventually accreted to the margin, coinciding with the onset of Gondwanan subduction (Fig. 1a) (Hervé et al., 2016, 2018).

If there was a passive margin during the Silurian-Early Devonian, the transition to subduction initiation occurred between 345 and 335 Ma (Bahlburg et al., 2009; Heredia et al., 2016; Creixell et al., 2021), although subduction-related magmatism and metamorphism are recorded from around 330-320 Ma (e.g., Hervé et al., 1988; Bahlburg and Hervé, 1997; Willner et al., 2005; Hyppolito et al., 2014a; Creixell et al., 2025). The first stage of the Gondwanan cycle (Pennsylvanian) is characterized by almost homogeneous behavior along the convergent margin (24°–38°S), with accretion, metamorphism, and magmatism occurring in different segments along the margin (Fig. 1b) (Díaz-Alvarado et al., 2019 and references therein). This stage is defined by the formation of frontal (Eastern Series) and basal (Western Series) units, with HP-LT metamorphic rocks preserved in the basal units. This first deformational phase is characterized by W to SW vergences (Willner, 2005; García-Sansegundo et al., 2014; Hyppolito et al., 2014a; Creixell et al., 2016; Fuentes et al., 2016).

The sedimentary protoliths of the Western and Eastern Series were deposited during the early Carboniferous, with slightly younger depositional ages for the underplated sediments of the Western Series. This indicates that the metasedimentary formations comprise units deposited during the passive margin stage and trench-fill sediments that fed the accretionary system (Hervé, 1988; Bahlburg and Breitkreuz, 1993; Heredia et al., 2017). Thermobarometric results from HP-LT rocks in the basal accretionary units show similar P-T trajectories between 28° and 39°S. Metamorphic peak conditions, determined in amphibolites and garnet mica-schist, reached up to 11 kbar and 700 °C, suggesting a high thermal gradient during the inception of the subductive margin (Willner, 2005; Willner et al., 2012; Hyppolito et al., 2015; Creixell

et al., 2016). North of 28°S, although there is concordance with the protoliths and ages of the metamorphic formations, no high-pressure rocks have been described in formations correlatable with the Western Series (Bell, 1987; Marioth and Bahlburg, 2003; Fuentes et al., 2016).

During the early Permian (Cisuralian), the western margin of Gondwana underwent a series of changes in tectonic activity, shifting to the foreland south of 34°S, and in the nature, volume, and location of magmatism, ending with the cessation of accretionary processes (Fig. 1c) (Díaz-Alvarado et al., 2019 and references therein). The segmentation of the margin and the significant differences observed in the fragments of the accretionary complex are associated with the asynchronous arrival of oceanic reliefs or ridges to the margin between 300 and 270 Ma, which also marks a peak in accretionary activity and a significant High Magma Addition Rate (HMAR) event in the arc north of 33°S (Creixell et al., 2025). To the south, the cessation of Cordilleran-type magmatism at 300–290 Ma approximately coincides with the end of the accretion of oceanic rocks to the margin (e.g., Hervé et al., 1988; Hyppolito et al., 2014a; del Rey et al., 2016), and the pervasive deformation of plutonic rocks around 33°–33°30' S (Webb and Klepeis, 2019). The oceanic rocks in the accretionary complexes show similar geochemical characteristics, mostly E-MORB metabasites, but have different tectonic relations with the metasedimentary formations, either as tectonic slices in the Western Series or as obducted and frontally accreted units (Fig. 1c) (Fuentes et al., 2018; García-Sansegundo et al., 2014; Hyppolito et al., 2014b).

The late Paleozoic subduction under the southwestern margin of Gondwana is characterized by oblique NE-directed convergence in these areas where this parameter was obtained (e.g., Kleiman and Japas, 2009; Fuentes et al., 2019). Some authors propose a shift in the margin direction from N-S to NNW-SSE around 34°S (Kleiman and Japas, 2009). The angular relation between the convergence direction and the margin azimuth has implications for the flow trajectories of underplated particles and other kinematic parameters associated with transpressional zones, as will be discussed later in light of the structural analysis results.

3. Structural characteristics of the Las Tórtolas Formation and the Chañaral mélange

One of the northernmost late Carboniferous metamorphic complexes exposed along the north and central Chilean coast (≈26°-39°S) is the Chañaral tectonic mélange, which belongs to the western domain of the Las Tórtolas Formation (Ulricksen, 1979; Bell, 1982) (Fig. 2a and b). Three domains have been distinguished in the Las Tórtolas Formation (Fuentes et al., 2019), from west to east: the Chañaral mélange facies, the volcanic domain, and the eastern series or eastern metaturbiditic unit (Fig. 2b). These units include sandstones and shales, as well as minor amounts of limestones, pelagic cherts, and conglomerates. Deep-sea basin-plain depositional environments have been interpreted for these associations (Bell, 1982). Basaltic rocks show E-MORB geochemical affinities. Metamorphic conditions are in the range of 350–400 °C, from greenschist and pumpellyite–actinolite facies for the mélange unit (Miller, 1970; Aguirre et al., 1972) to prehnite–actinolite facies for the eastern series (Marioth, 2001). Indeed, Marioth and Bahlburg (2003) estimated pressure conditions between 2 and 2.8 kbar at 300–350 °C for metapelites of the Chañaral mélange, based on the crystallographic b-parameter in white micas from this complex. No high-pressure metamorphic associations have been described in Las Tórtolas Formation, which contrasts with other late Paleozoic basal accretionary complexes in Chile where high-pressure rocks appear as stacked tectonic slices (e.g., Hyppolito et al., 2014a).

The structure of the eastern and central (volcanic domain) units is similar, consisting of N160°E to N-S trending, W- to SW-vergent, kilometric scale thrusts and associated fault-propagation folds (Fig. 2b and cross-section A-A'), with a NE to E dipping, axial-plane foliation mainly observed in the phyllite layers. In particular, the volcanic domain has been interpreted as an oceanic ridge or group of seamounts accreted during the Permian to the eastern unit (frontal accretionary formation) (Fuentes et al., 2018). In contrast, the Chañaral mélange domain shows an intense disruption of the sedimentary sequence, with a block-in-matrix structure conformed by centimetric to decametric quartzite blocks in a phyllitic matrix. It is, therefore, a tectonic mélange (e.g., Festa et al., 2019). According to its lithological and structural characteristics, the mélange domain has been described as generated in the shallow segment of a subduction plate boundary or located at the basal zone of an accretionary complex (Fuentes et al., 2016, 2018). This tectonic interpretation of the Chañaral mélange makes it an essential unit for the kinematic study of the late Paleozoic accretionary complex in the southwestern margin of Gondwana. Consequently, the results obtained by Fuentes et al. (2016, 2019) on its structure and kinematic interpretation are summarized below.

The structure of the Chañaral mélange is defined by the elongate, deformed shape of the quartzitic blocks and the fabrics developed in the phyllitic matrix (foliations and lineations), which constitute N-S-striking, linear (L) and linear-planar (L-S) domains (Fig. 2d). The quartzitic

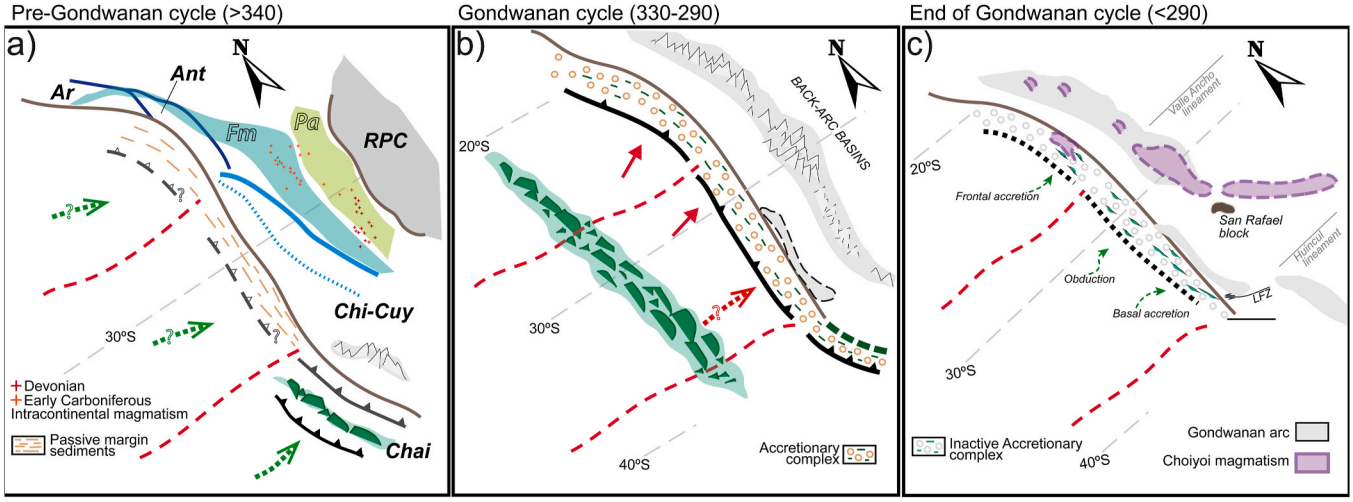

Fig. 1. - Sketch of the Devonian to Triassic tectonic evolution in the southwestern margin of Gondwana. The figure aims to synthesize the main hypotheses and margin configurations proposed over the past decades (see Section 2 for further details). Key: RPC: Rio de la Plata cratón; Pa and Fm: Pampean and Famatinian orogens; Ar, Ant and Chi-Cuy: Arequipa, Antofalla and Chilenia-Cuyania terranes; Chai: Chaitenia oceanic arc; LFZ: Lanalhue Fault Zone.

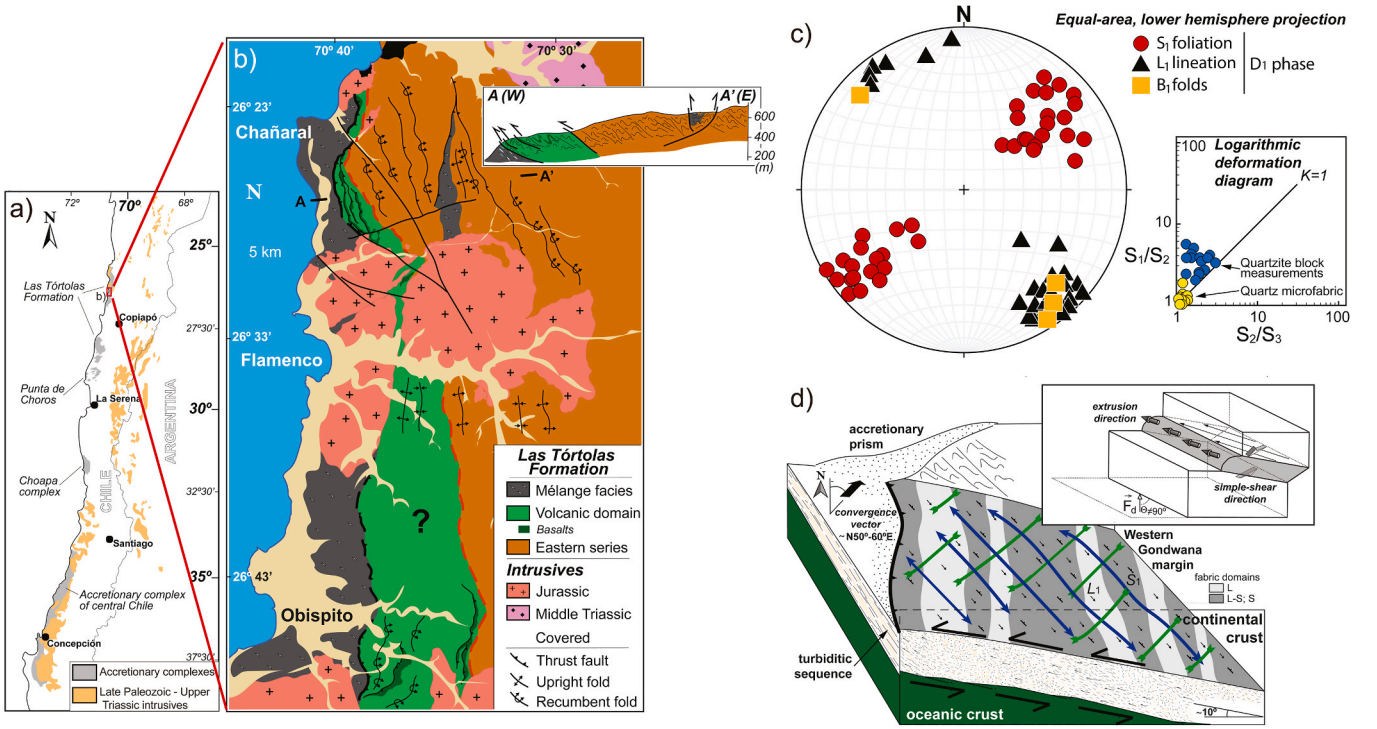

Fig. 2. - Summary of the data and results obtained in the study of the Chañaral mélange by Fuentes et al. (2019) by applying a transpression kinematic model. (a) Sketch showing the location of the main Paleozoic accretionary complexes and Late Paleozoic-Upper Triassic intrusive rocks in Chile and W Argentina. (b) Detailed geological map of the Chañaral region, including a geological cross-section (A-A′) of the three main units that form the Las Tórtolas Formation. (c) Spherical projection of the main structural elements (foliations, lineations and fold axes) in the Chañaral mélange, and shape of the finite strain ellipsoids projected on a logarithmic deformation diagram. (d) Block diagram illustrating the geometry and kinematics of the subduction channel in which the Chañaral mélange was generated. The blue (attractor) and green (repulsor) double-headed arrows indicate the flow apophyses. The inset shows the orientation of some of the main kinematic elements. See the main text for more details.

blocks show constrictional shapes within the L domains (Fig. 2c, logarithmic deformation diagram), where the foliation is poorly defined in the phyllite matrix. Lineations defined by the long axes of the quartzitic blocks are NW-SE-trending, shallowly plunging to the NW and SE (Fig. 2c, L_1 lineation). In contrast, L-S domains are characterized by less constrictional quartzitic blocks and a prominent foliation (S_1) in the phyllitic matrix. Foliation S_1 strikes NW-SE, dipping to the NE and SW (Fig. 2c). Isoclinal intrafolial folds have also been described, whose hinge lines parallel L_1 (Fig. 2c). Kinematic criteria show a predominant reverse-dextral displacement for the simple-shearing component of the deformation zone responsible for the Chañaral mélange. A predominantly constrictive coaxial component was also present during the activity of that deformation zone.

A 3D kinematic model has been applied to the Chañaral mélange by Fuentes et al. (2019), based on the model of triclinic transpression with inclined extrusion of Fernández and Díaz Azpiroz (2009). The deformation zone (supposed subduction channel) was oriented N-S to NNW-SSE, dipping to the E. Among the main results and interpretations of the use of the kinematic model in the Chañaral mélange are the following:

a.- The almost orthogonal arrangement between the vorticity normal section (including the simple-shear direction) and L_1 (inset in Fig. 2d).

b.- The estimated extrusion direction shows a low pitch on the boundary of the deformation zone (blue, double-headed arrows in Fig. 2d). Accordingly, particle transportation followed trajectories that were sub-parallel to the direction of the plate margin, preventing upward displacement of HP rocks in the accretionary complex. Material particles covered longer distances parallel to the plate boundary than along its dip direction before being underplated at the base of the accretionary wedge (see also Bell, 1987). Ultimately, this kinematic setting also explains the metamorphic conditions recorded in the Chañaral mélange.

c.- According to the previous result, an important tectonic flux of materials sub-parallel to the plate boundary is deduced in this case. Therefore, the estimated particle paths crosscut the vertical plane normal to the azimuth of the plate boundary (Fig. 2d; double-headed arrows). Consequently, 2D approximations to the flow within the subduction channel and accretionary wedge are not acceptable for the studied zone.

d.- A complex strain-partitioning pattern was produced, with the L domains corresponding with the low vorticities (flow dominated by the coaxial component; light grey bands in Fig. 2d), while the L-S or S domains appear for higher vorticities (flow dominated by the non-coaxial, simple-shearing component; dark grey bands in Fig. 2d). The boundaries between L-S and L domains are sub-parallel to the old plate boundary. This vorticity partitioning can be related to local rheological differences, or to the heterogeneous geometry of the zone (e.g., slight variations in the orientation of the deformation zone along or across its strike).

e.- The simple-shearing component associated with the plate convergence was particularly localized at the volcanic (central) and metaturbiditic (eastern) units (the supposed accretionary complex), as well as along the mélange domains with higher vorticities. However, most of the coaxial component was focused on the mélange (the supposed subduction channel).

f.- The trend of the convergence vector deduced for the blocks separated by the deformation zone is N50°-60°E (Fig. 2d). Therefore, an

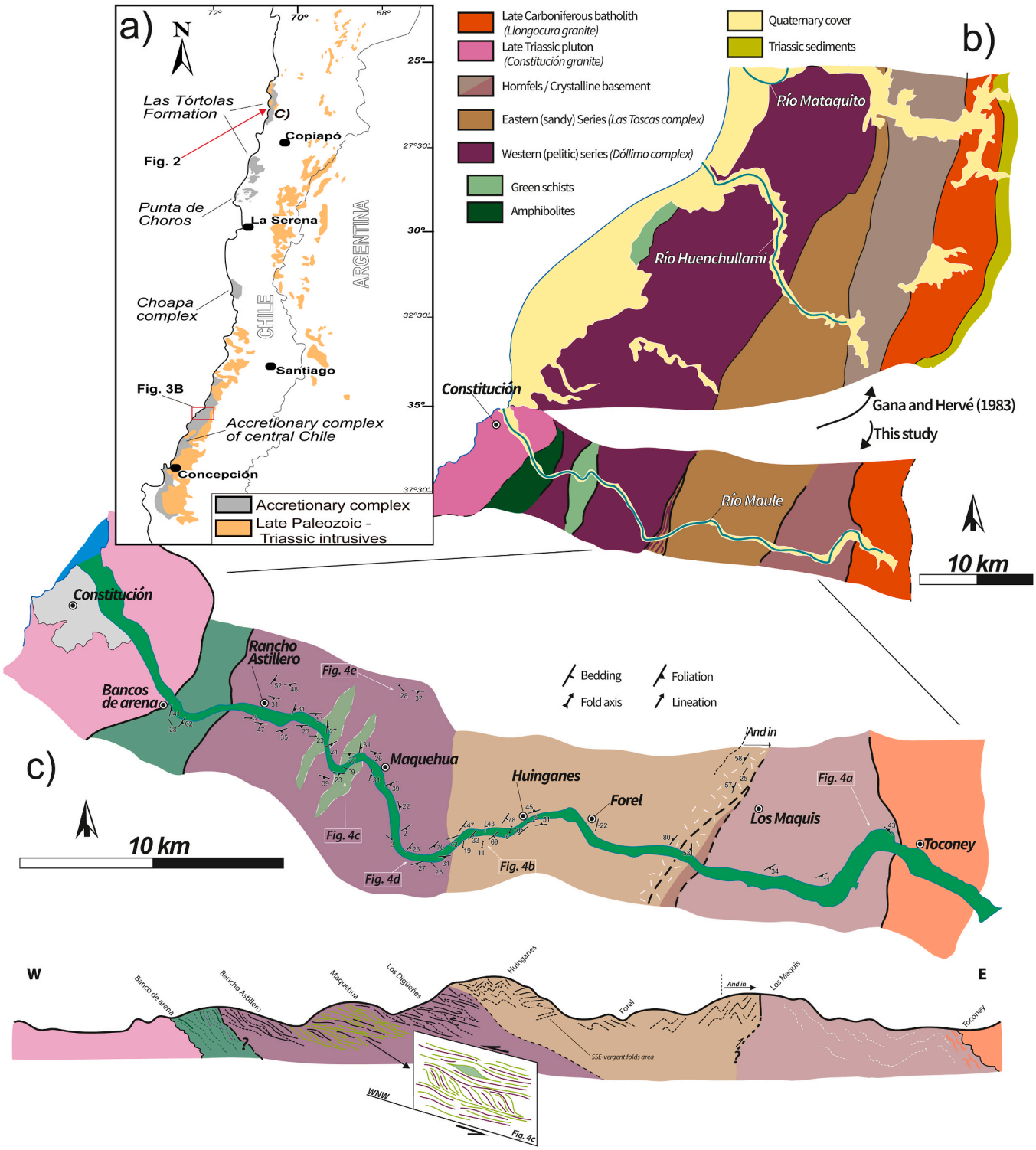

Fig. 3. - A) Map of western South America showing the distribution of the late Paleozoic accretionary complex fragments along the Chilean coast and the late Paleozoic to Upper Triassic magmatism associated with the convergent margin (modified from Fuentes et al., 2019). The detailed maps in Fig. 2 (Las Tórtolas Formation) and 3b (Maule section) are indicated in the figure. B) Detailed map of the study area (Maule section) and the northern area mapped by Gana and Hervé (1983). The figure shows a good correlation between recent observations (this work) and those made in the 1980s. C) Detailed map and cross-section of the Maule river area. The locations of the outcrops shown in Fig. 4 are indicated on the map. The main locality (Constitución) and the railway stations are marked for reference.

oblique convergence tectonic setting is deduced for the late Paleozoic subduction in northern Chile.

g- A second deformation phase (D_2) folded S_1 and L_1, and has been interpreted as due to the arrival of submarine reliefs (volcanic central domain), which did not entail any important change in the direction of convergence between the blocks and plates involved.

h.- Despite the limitations imposed by the kinematic model used (see Fuentes et al., 2019 for a more detailed explanation), the results are robust, highlighting the importance of performing 3D kinematic studies in tectonic mélanges. In this work, a comparison is made between the

Chañaral mélange and similar units to the south in order to obtain a more complete tectonic picture of the activity and characteristics of the entire subduction system during the Late Paleozoic.

4. Structural and kinematic analysis of the Carboniferous accretionary complex in the Maule-Concepción area

4.1. Lithological and metamorphic characteristics of the rocks comprising the Maule section

The studied section of the Coastal Accretionary Complex of Central Chile (Fig. 3a) extends from the late Carboniferous batholith, composed of granites, granodiorites and tonalites, located approximately 30 km west of Talca, to the coast at Constitución, following the Maule River (Fig. 3b and c). Additionally, observations have been made in similar and correlatable units along the coast and south of Concepción. In the absence of high-pressure rocks within the analyzed lithological units, the assignment of these lithologies to the Western or Eastern Series has been based on the intensity and style of deformation, as well as the presence of oceanic-derived rocks (metabasites). According to the mineralogical associations studied in the rocks described below, the metamorphic conditions do not exceed the greenschist facies, except for those rocks within the metamorphic aureole of the intrusive bodies, which record the corresponding temperature increase (Gana and Hervé, 1983; Willner, 2005; Hyppolito et al., 2014a). The nomenclature for certain formations and structures in the study area follows the works of García-Sansegundo et al. (2023), Gana and Hervé (1983), and recently Jorquera et al. (2023). The map from Gana and Hervé (1983) is shown in Fig. 3b to highlight the consistency and continuity of our observations.

4.1.1. Carboniferous plutonic rocks and the crystalline basement

The intrusive rocks constituting the Gondwanan arc in this segment are primarily composed of calc-alkaline tonalites, granodiorites and monzogranites, with minor occurrences of diorites and two-mica granites (e.g., Hervé et al., 1988; Deckart et al., 2014; Jorquera et al., 2023; Creixell et al., 2025). Magmatic fabrics are well recognized along tonalites and granodiorites in the Concepción area (37–38° S; Steenken et al., 2022) but are rarely developed along the Maule section where monzogranites are the dominant lithology (35° S). U-Pb geochronological results indicate that the batholith was constructed between 322 and 300 Ma and is notably devoid of well-defined Permian magmatism (Gana and Tosdal, 1996; Godoy and Loske, 1988; Deckart et al., 2014; Velásquez et al., 2024). While its compositional and geochemical characteristics are similar to the late Carboniferous magmatism further north, this segment (33–38° S) is distinguished by the proximity of the arc to the metamorphic rocks constituting the accretionary complex (Fig. 3a) and by the extent of the contact aureole defined around the batholith, approximately 20–40 km in width (Hervé, 1977; Willner, 2005).

Intrusive rocks are in contact with a crystalline basement, here differentiated from the Eastern Series, composed of migmatites, paragneisses, and pelitic schists that exhibit local melting features in mm-scale veins (Fig. 4a). Leucosomes are hosted by granoblastic rocks composed of quartz, biotite, andalusite, fibrous sillimanite, spinel and poikilitic muscovite and cordierite. The protolith of the metamorphic host rocks of the Carboniferous batholith has traditionally been associated with parts of the Eastern Series, which were affected by a regional-scale thermal aureole, with successive sillimanite, andalusite and biotite mineral zones distributed parallel to the intrusive contact with increasing distance to it (e.g., Hervé, 1977). In the Maule section, the crystalline basement comprises a section of ca. 7–10 km, notoriously smaller than the 50 km thick thermal aureole proposed by Hervé (1977) in the Nahuelbuta section (37°–38° S).

4.1.2. Eastern series

This domain comprises a succession of low-grade phyllites and quartzites. Only in proximity to the contact with the crystalline basement the phyllites exhibit prismatic and poikilitic andalusite and acicular sillimanite crystals (2–3 cm in length) that postdated the main foliation (Fig. 3c). This unit corresponds to the Eastern Sandy Series (García-Sansegundo et al., 2023) and the Las Toscas Complex (Gana and Hervé, 1983; Jorquera et al., 2023). The phyllites consist of a lepidoblastic aggregate of biotite and white mica alternating with fine bands of quartz with granoblastic texture. The quartzites contain a minor percentage of white mica, biotite, and iron oxides (Gana and Hervé, 1983). Lithologically monotonous, the structural characteristics define several domains based on the vergence of mostly close to tight, asymmetrical to overturned folds (Fig. 4b). In the eastern part, near the batholith and its basement, the structures verge eastward, while W-NW vergences dominate in the rest of the metasedimentary unit. East of the Huinganes station, there is a domain approximately 500 m wide with S-SE vergences (Fig. 3c). Low pressures of metamorphism are generally deduced from the mineral assemblages of the Eastern Series at the Maule section, which is consistent with P-T calculations around 2.5–3.0 kbar for one sample of these rocks collected at Huinganes station (Willner, 2005).

4.1.3. Western Series: Pelitic unit, green schists and amphibolites

Between the Huinganes and Maquehua stations (Fig. 3c), the metaturbidite succession gradually loses its psammitic component. As this lithological change becomes evident, the tight, overturned folds are predominantly replaced by isoclinal folds, with additional structures such as S-C fabrics and asymmetric objects developing particularly in quartz exudates intercalated within the metapelitic rocks (Fig. 4c–e). Irregularly spaced crenulation cleavage affecting the main foliation is also observed around Maquehua station. This unit corresponds to the Eastern Pelitic Series (García-Sansegundo et al., 2023) and the Dóllimo Complex directly north of Maule river (Gana and Hervé, 1983). Besides the deformation style, the fabric orientations also change between the Eastern and Western series. The N-S to N30°E preferred orientations of the Eastern Series alternate in this pelitic domain with E-W to N110°E-directed foliations, exhibiting very low dips (Fig. 3c).

The pelitic domain transitions from east to west from phyllites to medium-grained schists, which are spotted by the appearance of albite crystals. These nodular schists can contain up to 40 % albite, along with smaller percentages of quartz, white mica (phengite), pre-D2 garnet and locally some graphite-rich bands (Gana and Hervé, 1983; Willner et al., 2005; García-SanSegundo et al., 2023). Chlorite-rich metabasites crop out from the central zone to the west of the pelitic unit (Fig. 3c), where they intercalate with the schists in centimeter-scale bands (Fig. 4c). Similar bodies of greenschists have been described west of the Dóllimo Complex (Fig. 3b). They are composed of amphibole, epidote, chlorite, and albite, with lesser amounts of quartz and white mica (Gana and Hervé, 1983). The rheological contrast between the centimeter-scale bands of greenschists and pelitic schists allows for the observation of lineations, numerous S-C structures and asymmetric objects, whose kinematic indicators clearly show a WNW vergence (Figs. 3c and 4c, d).

A tabular body of amphibolites occurs west of the pelitic schists. These are fine-grained amphibolites with epidote-rich bands. Amphibolites present asymmetric albite porphyroblasts and locally abundant titanite and epidote. To the west, metamorphic rocks are affected by the presence of a Triassic intrusive body (Fig. 3b and c). Towards the contact with the pelitic schists, the massive amphibolites alternate with pelitic schists.

Between the Maule and Mataquito rivers, in addition to greenschists and amphibolites, small bodies of metacherts, marbles, and serpentinites have been described, included in the pelitic matrix that constitutes the Western Series (Gana and Hervé, 1983). The association of this pelitic unit with the Western Series is based on the presence of intercalations of greenschists, amphibolites, and ultrabasic rocks derived from oceanic rocks, the style and intensity of deformation, and the fundamentally pelitic composition of the matrix. The entire coast from Constitución to Concepción presents this type of schists with albite porphyroblasts, with

(caption on next page)

Fig. 4. - Photographs of the main units in the Maule river section. The locations of these observations are indicated in Fig. 3c. A) Migmatites forming part of the crystalline basement of the Carboniferous batholith. B) Minor folds in the succession of phyllites and quartzites (Eastern Series) with westward vergence. The axis of this fold dips 19° towards N189E, representing most folds in the western part of this unit. C) Domain of metabasites (greenschists) intercalated with pelitic schists of the Western Series. White arrows indicate some of the abundant structures with kinematic indicators (S-C structures and asymmetrical objects) observable in this domain. The orientation of the measured lineations at this outcrop is shown alongside the north indication in the image. D) Inclined, westward-verging folds in the eastern metaturbidite succession are replaced by S-C structures and isoclinal folds in the pelitic series dominating the western domain of the section. E) Pelitic schists with abundant quartz exudates and tight to isoclinal folds verging W-NW in the Western Series. F) Appearance of the same schists on the coast of Concepción, approximately 200 km south of the study area.

very low dip of the foliation and W-NW vergence of the structures (Fig. 4f). Further north, in Pichilemu (ca. 34°20' S), these same units include tectonic slices that record high pressure and low to medium temperature (blueschists, garnet-mica schists, and amphibolites) (Willner, 2005; Hyppolito et al., 2014a; Muñoz-Montecinos et al., 2020).

Metamorphism of the pelitic schists and metabasites at the Maule section registered peak metamorphic conditions with pressures around 9 kbar and greenschists facies temperatures <430 °C, similar to those observed further north at 34° S (Willner, 2005), but with absence of blueschist and garnet schists like those described at Pichilemu and Punta Sirena, respectively (Willner et al., 2005; Hyppolito et al., 2014a). Prograde metamorphism was followed by retrograde conditions around or below 280 °C and shallow depths (~8 km), during a first stage of exhumation of the accretionary prism (Willner et al., 2005).

4.2. Structural characteristics

The Carboniferous Coastal Accretionary Complex in the Maule area includes a belt of strongly deformed rocks, with a NE-SW strike and gently to moderately dipping towards the SE (Fig. 3). Structurally, the

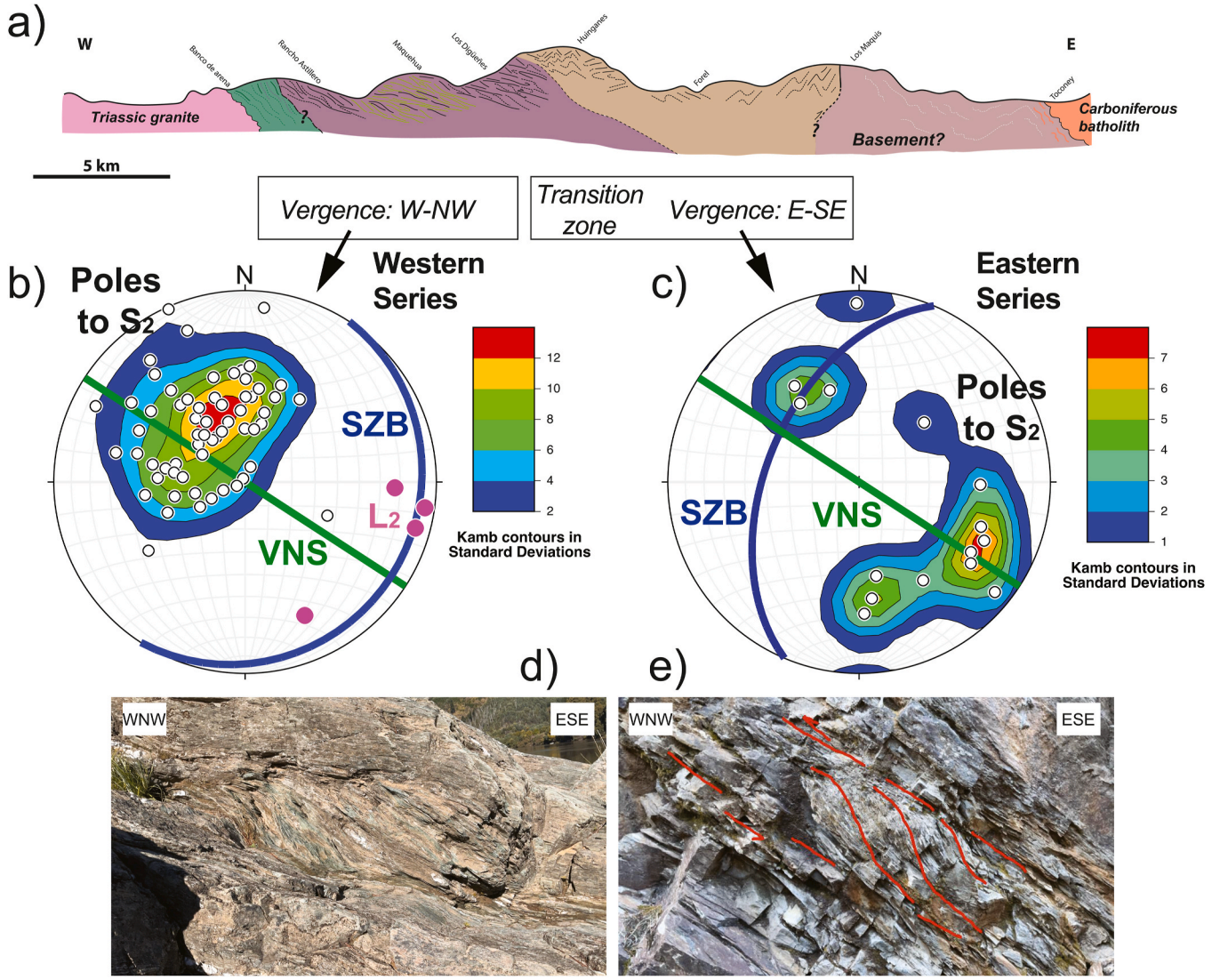

Fig. 5. - (a) Geological cross-section of the accretionary complex in the Maule River. (b) Equal-area, lower hemisphere projection of the poles to the main foliation (S), and lineations (L) in the Western Series (W-vergent domains) of the Maule section. VNS and SZB stand for vorticity normal section and shear zone boundary, respectively. The density contours of the S poles have been constructed using the Kamb method, with E = 2σ. (c) Same as in (b) for the Eastern Series (E-vergent and transitional domain data). Kamb method, with E = 1σ. In this and the following figures, the Stereonet software (Allmendinger et al., 2012) has been used for the spherical projections. (d) Composite planar fabrics and other asymmetric indicators in metabasites (green schists) of the W-vergent domain. Section of maximum asymmetry (VNS). Top-to-the-WNW. (e) Idem in the W-vergent domain phyllites.

Maule River section includes two well-differentiated sectors (Fig. 5a). This was also highlighted by Gana and Hervé (1983) in a detailed study of the area located just north of the Maule River section. To the east, and in sub-vertical contact with high-grade metamorphic rocks (crystalline basement), there is a succession of phyllites and quartzites (Eastern Series) with structures (close to tight folds and associated foliation) that shows opposed vergences: to the E-SE in the eastern area and to the W-NW in the central and western areas of this unit (Fig. 3c and d). In contrast, the pelitic unit (Western Series), which also includes greenschists and amphibolites, shows different structural patterns: isoclinal folds, abundant S-C structures, and presents constant N to NW vergences. In these latter domains, a mineral and stretching lineation trending NW-SE with low plunges towards the E and SE is observed (Fig. 5b). The best and most abundant kinematic criteria are observed in WNW-ESE, sub-vertical trending planes, and consistently indicate top-to-the-WNW displacement (Fig. 5d and e), although Richter et al. (2007) described local criteria indicating top-to-the-ESE shear senses, particularly in the westernmost part of the Maule section.

According to Richter et al. (2007), S_1 is an axial-plane foliation of folds affecting the S_0, vergent to the E especially in the eastern part of the Eastern Series. On the other hand, the S_2 foliation is predominant in the zone of W-vergent structures, both in the Eastern and Western Series, and tends to show low to moderate dips both towards the SE and towards the NW. Up to three deformation phases (D_3 to D_5) subsequent to the main one have been described in the region (Gana and Hervé, 1983), although their low penetrativity and intensity and their marked heterogeneity mean that their effects on the orientation of the previous structures and fabrics are local and apparently scarce. Indeed, the D_3 folds, are usually local and less penetrative than those of D_2, although in the Western Series, Richter et al. (2007) described $S_{2\text{-}3}$ and $L_{2\text{-}3}$ planar-linear fabrics. The foliation used in this work for the structural analysis of both structural sectors (E-vergent and W-vergent) mainly corresponds to the S_2 of Richter et al. (2007; their Figs. 3 and 5) and Gana and Hervé (1983; their Figs. 11 and 12), while the lineation measured in the W-vergent sector coincides with their L_2 (and $L_{2\text{-}3}$) lineation. The orientations of the main foliation and the associated lineation measured by Richter et al. (2007) in the Maule River section, and by Gana and Hervé (1983) north of that section, statistically coincide with those of Fig. 5b and c, including the greater variability of the main foliation in the Eastern Series (note that a large sector of the eastern part of the Eastern Series of Richter et al., 2007, corresponds to what is considered in this work as crystalline basement). Therefore, this work mainly describes the effects of the D_2 phase of Gana and Hervé (1983) and Richter et al. (2007), which is the main and most penetrative phase in the entire region. According to these authors, the D_1 phase is almost completely transposed in the Western Series, and is strongly affected by the folds and foliation of the D_2 phase. However, D1 is important in the easternmost part of the Eastern Series, and the east-verging folds may show a continuous activity of phases D1 and D2. In turn, as previously indicated, phase D3 may be locally significant in the Western Series, with a progressive deformation between phases D2 and D3 being observed.

In the case of the Chañaral mélange, the subduction channel was considered by Fuentes et al. (2019) to be equivalent to a large shear zone, so it was possible to successfully simulate the flow within it using a transpression kinematic model. The same argument can be applied to the southern accretionary complex represented by the Maule River transect. However, there are two features that differentiate the Maule section from the Chañaral one. The first is that there are no constrictive fabrics (L or L-S) in the Maule River region, but they tend to be plano-linear. Second, the Maule section is characterized by two distinct domains with contrasting vergences, as explained above. Therefore, both domains have been considered separately here. In order to evaluate the kinematic evolution of the accretionary complex of the Maule River, a brief methodological presentation of the kinematic model used will first be made, and then the application of the model in the two domains (W- and E-vergent) of the Maule section will be detailed.

4.2.1. Methodology of kinematic analysis

From a strictly kinematic point of view, transpression zones are considered as deformation volumes of rock affected by simple shear and a component of shortening across the zone, therefore simultaneously combining a coaxial and a non-coaxial component (e.g., Fossen and Tikoff, 1998). The general analytical model of transpression described by Fernández and Díaz Azpiroz (2009) has been used in this work. This model considers a homogeneous, steady, and volume-constant flow, with a non-coaxial, simple-shear component parallel to the shear zone boundary, and a coaxial component (not necessarily pure shear) with shortening normal and stretching parallel to the shear zone boundary. The simple-shear component may be oblique relative to the strike of the shear zone boundary (angle of obliquity, ϕ, or pitch angle of the simple shear direction on the shear zone boundary; e.g., Lin et al., 1998). The direction of maximum infinitesimal stretching of the coaxial component -extrusion direction-forms an angle υ (extrusion obliquity) with the dip direction of the shear zone boundary (e.g., Fernández and Díaz Azpiroz, 2009). The flow vorticity measures the ratio between the coaxial and non-coaxial parts of the flow, and is approximated in this work with the Truesdell kinematic vorticity number W_k (Truesdell, 1953). W_k is independent of the simple-shear (ϕ) and extrusion (υ) obliquity angles. Values of W_k range from 0 for coaxial flow to 1 for simple shear. The general shape of the infinitesimal ellipsoid of the coaxial component is defined by its logarithmic shape parameter K, with $K = 1$ (plane strain, pure shear) separating flattening ($K < 1$) and constrictional ($K > 1$) geometries. The modeled flow therefore depends on four main variables, ϕ, υ, W_k and K, which describe the spatial distribution of the velocity field of the body (the velocity gradient tensor). The eigenvectors of the velocity gradient matrix are called flow apophyses (e.g., Passchier, 1997). For the transpression model presented by Fernández and Díaz Azpiroz (2009) two of the flow apophyses are in the shear plane, while the third apophysis is commonly oblique to it. The oblique apophysis coincides with the orientation of the vector of relative displacement between the blocks separated by the shear zone, and it can be termed convergence direction (Fossen and Tikoff, 1998).

Therefore, in this work, the equations of Fernández and Díaz Azpiroz (2009) have been used to simulate the shape and orientation of the principal axes of the finite deformation ellipsoid. The results predicted by the model have been investigated for a wide range of values of ϕ, υ, W_k and K. These results include, for each combination of these four parameters, the shape of the finite deformation ellipsoid (plotted in a logarithmic deformation diagram), and the orientation of its three principal axes ($X \geq Y \geq Z$). The results of the analytical model have been rotated according to the orientation of the boundaries of the deformation zones in the Maule section, and have been compared with the natural fabrics (foliations and lineations). In this respect, the orientation of the foliation poles can be compared to that of the Z axis of the finite deformation ellipsoid, while the lineations coincide with the X axis of the ellipsoid (on the complex relationships between the principal axes of the finite deformation ellipsoid and natural tectonic fabrics, see, e.g., Williams, 1976; Ramsay and Huber, 1983; Fossen, 2016). The results of the model that best fit the natural fabrics visually (in stereographic projection or in the logarithmic deformation diagram) are used to constrain the values of the model parameters (ϕ, υ, W_k, K) and, therefore, to kinematically characterize the studied shear zones. Regarding the angle ϕ, its approximate value can be obtained by establishing the orientation of the plane known as the vorticity normal section (VNS), which is the section in which the maximum asymmetry or the greatest number of unequivocal kinematic markers (S/C, C′, porphyroclast systems, asymmetric folds and boudins, among others) are observed. The angle ϕ would be given by the pitch on the shear zone boundary of the intersection line between the VNS and the shear plane itself (e.g., Díaz Azpiroz et al., 2019).

The natural structural data we used to check the kinematic model are

the following: (1) For the whole Maule River section (W-vergent and E-vergent domains), new data taken in this work on the orientation of foliation and tectonic lineation (essentially S_2 and L_2), represented in Fig. 5. (2) For the W-vergent domain, data on the orientation of the tectonic lineation and the shape of the finite strain ellipsoids measured by Richter et al. (2007) in the Maule River area. (3) For the E-vergent domain, the orientation of the long axis (X) and the shape of the finite strain ellipsoids measured in the Maule River area by Richter et al. (2007).

Finally, the results of this fit between model and reality allow the estimation of the direction of convergence (oblique apophysis) between the blocks separated by the shear zones.

4.2.2. W-vergent domains

The strike of the main lithological contacts in this area is between N030°E and N035°E. Therefore, an intermediate value of N033°E has been considered for the strike of the shear zone boundary (SZB). Furthermore, a preliminary kinematic analysis considering more N-S azimuths has failed to explain the orientation of the foliation and lineation measured in the field. Regarding the dip of the SZB (10°SE), it is similar to that considered in Chañaral. Although Willner (2005) estimated a subduction angle of 25° using cartographic and metamorphic considerations, dips larger than 10° have been explored in this work with poor results. It is possible that the entire region has undergone a rigid rotation during post-Paleozoic tectonic history, or that the considerations of Willner (2005) are not completely applicable to the case of the Maule River section. Concerning the vorticity normal section (VNS), field observations indicate that sections with the highest asymmetry are sub-vertical and show an average azimuth of N0123°E (Fig. 5d and e). The simple shear direction results from the intersection between the VNS and the SZB. This intersection occurs according to the dip direction of the SZB (Fig. 5b), so the pitch of the simple shear direction on the SZB plane (angle ϕ) is 90°. This means that the non-coaxial component characterizes the shear zone as a thrust.

In this case, abundant information is available regarding finite-strain data, obtained by Richter et al. (2007) by studying metagreywacke and phyllosilicate-rich levels using the R_f/ϕ technique and X-ray texture goniometry, respectively. The results by Richter et al. (2007) show a wide variety of finite-strain ellipsoid geometries, from the constriction to the flattening field. Classical kinematic models show that it is not possible to obtain constrictional ellipsoids under transpression (e.g., Fossen and Cavalcante, 2017). By applying the general triclinic transpression model of Fernández and Díaz Azpiroz (2009), Fuentes et al. (2019) showed that the constrictional finite-strain ellipsoids obtained in the Chañaral mélange could be simulated assuming that the coaxial flow component deviates from the pure shear and enters the constriction field. Therefore, in this work, it was preferred to consider a range of values for the shape parameter (K) of the infinitesimal ellipsoid of the coaxial component, including the possibility of coaxial components in the constriction field ($K > 1$).

The extrusion direction (direction of maximum infinitesimal stretching of the coaxial component, which forms an angle υ with the true dip line of the SZB) usually coincides with the dip of the SZB (i.e., $\upsilon = 0°$). However, in order to better explain the fabric orientation and finite-strain data, the following values of angle υ have been investigated: 0°, 90° (horizontal extrusion), 60° (pitch of 30°NE), and 120° (pitch of 30°SW). Finally, a wide range of values of the kinematic vorticity number (W_k, Truesdell, 1953) has been tested in the interval between 0 (coaxial flow) and 1 (simple shear): 0.2, 0.4, 0.6, 0.81, 0.9, 0.95, 0.999.

From the wide range of parameter values that control the transpression model cited above, this work will show only those that have allowed an acceptable fit with the natural fabrics and with the finite-strain data estimated by Richter et al. (2007) specifically along the Maule River section. The transpression model yields an acceptable fit between the orientation of the foliation poles (S_2) and the Z (short) axes of the finite strain ellipsoid determined by the model for $\phi = 90°$ and $\upsilon = 60°$ and 120° (Fig. 6a, left). There is greater variability in the natural data, but the model predicts well the zone of greatest pole density. This variability may be due to different causes: the effect of later deformation phases (Gana and Hervé, 1983); the margin of error of each measurement; local variations in the orientation (strike and dip) of the SZB caused, for example, by the presence of bodies with complex, non-tabular geometry; local modifications in the orientation of the simple shear or extrusion component (due, for example, to the local presence of bodies that differ in competence with respect to the dominant lithology). Regarding the lineation, it is well predicted by the X (long) axes of the finite strain ellipsoids calculated by the model (Fig. 6a, left; also including a density diagram of the stretching lineation measured by Richter et al., 2007, their Fig. 5). In fact, the gently E-dipping lineations are well explained by the model for $\upsilon = 60°$ (E and NE plunging lineations) and 120° (S and SE plunging lineations), and a wide range of W_k values. Although the fit of the kinematic model to natural data allows some constraint of the value of W_k, it would be desirable in the future to perform independent determinations of vorticity by using appropriate techniques (e.g., Xypolias, 2010; Fossen and Cavalcante, 2017), mainly at the microscopic scale. A large fluctuation ($\geq \pm 60°$) of the extrusion direction around the actual dip of the SZB can explain all the lineation data. In all cases, the best fit is obtained with high values of K (=5, although larger values are also possible) for the coaxial component of flow. To better check and constrain these results, the shapes of the finite-strain ellipsoids determined by Richter et al. (2007) in the Maule River section (Western Series) have been represented in a logarithmic deformation diagram. The finite deformation trajectories predicted by the model (for $\upsilon = 60°$ and 120°) almost completely cover the variety of ellipsoid shapes determined from the natural samples (Fig. 6a, right). However, there are a couple of samples, located close to the line of the oblate ellipsoids, which cannot be explained by the model, unless a horizontal extrusion direction is considered ($\upsilon = 90°$), in which case, it is possible to account for all the estimated finite-strain ellipsoids (Fig. 6b, right). This monoclinic flow situation ($\phi = 90°$ and $\upsilon = 90°$) cannot be considered as the only possible one in the Maule River section, because it only accounts for some of the finite-strain ellipsoids, and it cannot explain the wide dispersion in the orientations of S_2 and L_2 (Fig. 6b, left).

Summarizing these results, the W-vergent zone of the Maule River section can be explained with a triclinic to monoclinic transpression kinematic model, with a constrictional coaxial component ($K = 5$) and with the simple shear direction acting parallel to the dip of the SZB. The extrusion direction fluctuated $\geq \pm 60°$ around the true dip of the SZB.

4.2.3. E-vergent domain

The SZB is assumed to have the same direction as in the W-vergent domains, but the dip here is towards the W. After a first analysis with a low dip (10°W), it has been observed that the model cannot explain the foliation data measured in the E-vergent domain. Therefore, higher dips have been considered. In this case, a modeled SZB with a dip of about 50°W seems to yield reasonable fits to the observed natural data. Thus, the orientation of the SZB would be: N033°E/50°W. The range of values of the orientation of the simple-shearing direction (angle ϕ; sense of displacement: reverse) and kinematic vorticity (W_k) is the same as that used in the W-vergent domain. Regarding the extrusion direction (angle υ), a wide range of values has been simulated, although the best results have been obtained for $\upsilon = 0°$ (monoclinic flow) and $\upsilon = 40°$ (pitch of 50°SW) and 140° (pitch of 50°NE) (triclinic flows).

In the E-vergent domain, only foliation data are available, not lineations. But it is possible to use the orientation of the long axes (X) of the finite-strain ellipsoids determined by Richter et al. (2007) in that domain (density contours with grey scale in Fig. 7, left). The ϕ and W_k values that allowed to explain the structure of the W-vergent domains also give good results in this case (Fig. 7, left). The main maximum in the orientation of the foliation poles (S_2) is well explained by the model

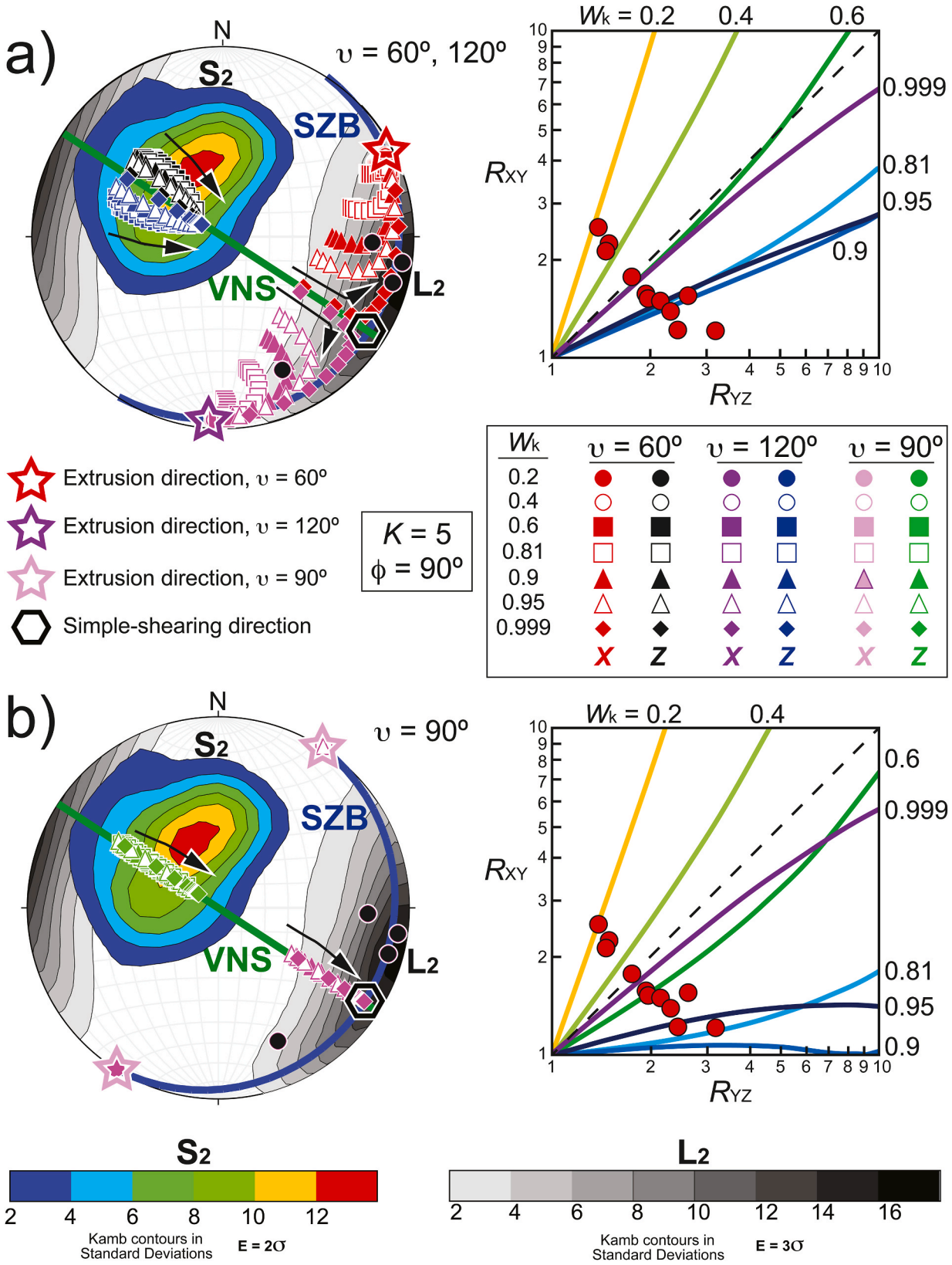

Fig. 6. - Results of the application of the transpression model to the W-vergent domains of the Maule section, showing acceptable fits between the model and the natural data for given values of the parameters controlling the model (ϕ, υ, W_k, K). Equal-area, lower hemisphere projections. To the structural data (L_2 and poles to S_2) of these domains, shown in Fig. 5b, the orientation predicted by the model for the long (X) and short (Z) axes of the finite strain ellipsoid for different values of vorticity (W_k) have been added, as well as the stretching lineations measured by Richter et al. (2007) in the studied zone, and represented as grey-shaded contours. The black arrows indicate the reorientation of the X and Z axes with increasing amount of finite strain. VNS: vorticity normal section. SZB: Shear zone boundary. a) Results for $\upsilon = 60°$ and 120°. b) Results for $\upsilon = 90°$. In both cases, to the right, logarithmic deformation diagrams with the strain trajectories predicted by the model (colored curves), and the finite strain-ellipsoids (red circles) measured by Richter et al. (2007) along the Maule River section (W-vergent domain), are shown.

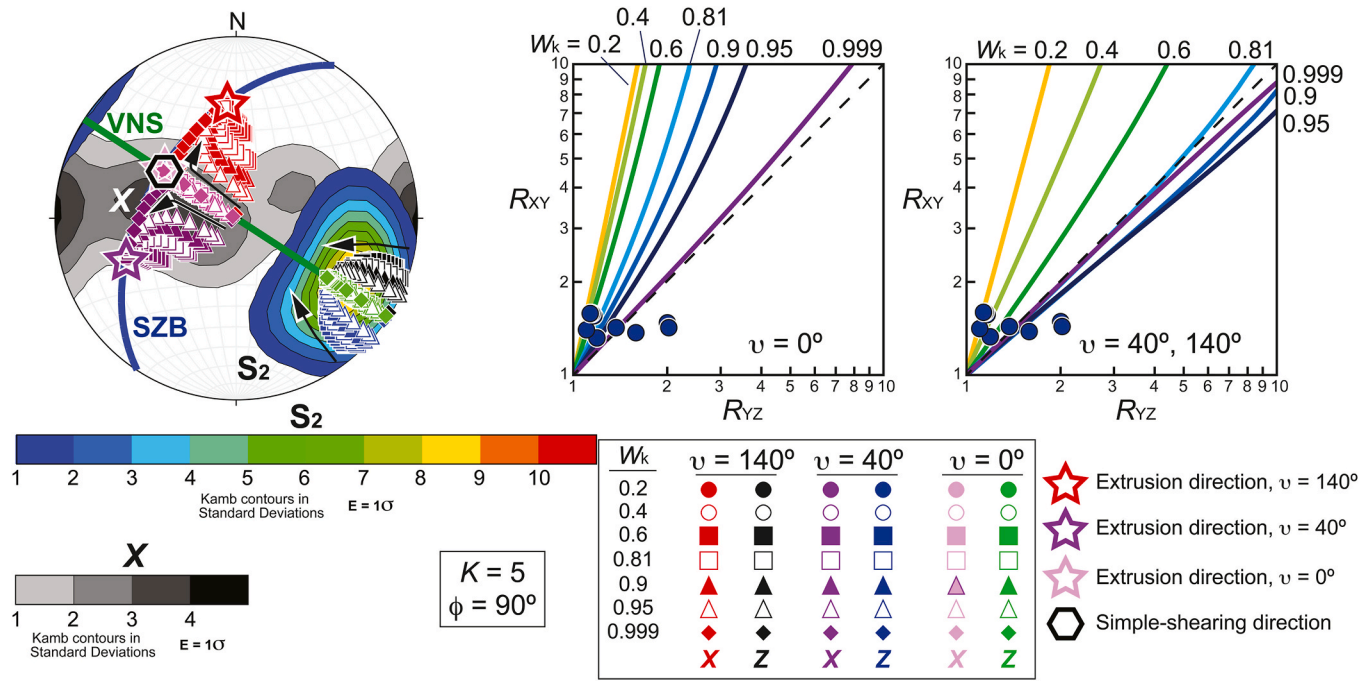

Fig. 7. - Results of the application of the transpression model to the E-vergent domains of the Maule section, showing acceptable fits between the model and the natural data for given values of the parameters controlling the model (ϕ, υ, W_k, K). Equal-area, lower hemisphere projection. To the structural data (poles to S_2 shown in Fig. 5b, and *long* axis of the finite-strain ellipsoids, X, determined by Richter et al., 2007, and depicted with grey-shaded contours), the orientation predicted by the model for the long (X) and short (Z) axes of the finite strain ellipsoid for different values of vorticity (W_k) have been added. The black arrows indicate the reorientation of the X and Z axes with increasing amount of finite strain. VNS: vorticity normal section. SZB: Shear zone boundary. Results for $\upsilon = 0°$, 40°, and 140°. To the right, logarithmic deformation diagrams with the strain trajectories predicted by the model (colored curves), and the finite strain-ellipsoids (blue circles) measured by Richter et al. (2007) along the Maule River section (E-vergent domain), are shown.

considering the variability of υ ($\pm 40°$ around the real dip of the SZB). There are two other minor maxima of S poles that are not predicted by the model. The first corresponds to the poles plunging towards the NW. It is very similar to the foliation orientation in the W-vergent domains. Therefore, it is possible to explain these data either as taken at the limit between both domains of opposite vergence, or as minor zones verging to the W within the general zone verging to the E. The second maximum, with poles inclined towards the S, is more difficult to explain and would require local variations in the orientation of the SZB or in the directions of simple shear or extrusion. The effect of later structures, especially the folds of phases D_3 and D_4 described by Gana and Hervé (1983), cannot be ruled out. One of the main maxima of the orientation of the X axes of the finite deformation ellipsoids determined by Richter et al. (2007) can also be explained with the model (Fig. 7, left). The same does not happen with the E-W, sub-horizontal maximum, which is not compatible with the orientation of the SZB considered. To explain this maximum it would be necessary to admit the local action of secondary shear zones with low dip, even subhorizontal. The shape of the finite-strain ellipsoids, which also fluctuates between the constriction and flattening fields in this domain, can be explained by the model, especially under triclinic flows (oblique extrusions with $\upsilon = 40°$ and 140°; Fig. 7, right). There are a couple of ellipsoids, within the flattening field, that would require larger fluctuations in the extrusion direction ($\upsilon \geq \pm 40°$). Although these values of υ could help to explain the shape of those ellipsoids, the orientation of the X and Z axes they predict fit poorly with the orientations of the long axes of the estimated finite-strain ellipsoids and the measured poles to S_2. Therefore, it is considered that, although flows with these values of υ may have acted, they should be subordinated with respect to the more common situations of $\upsilon \leq \pm 40°$.

Summarizing the results for the E-vergent domain in the Eastern Series, it can be fitted by a top-to-the-E, reverse shear zone ($\phi = 90°$), with high dip (50°W), with a wide range of kinematic vorticity (W_k) values, together with an extrusion direction (υ angle) that could fluctuate even more than 40° with respect to the true dip direction of the SZB. Again, the K value of the coaxial component must be located in the constriction field ($K = 5$, although larger values are also possible) in order to explain some of the strongly constrictional ellipsoids determined in the zone.

5. Discussion

5.1. Results of the structural analysis in the Maule river section of the Coastal Accretionary Complex of Central Chile

Looking at the Maule section (Figs. 3 and 5a) and taking into account the structural field observations and the great coherence in the kinematic results of the opposite vergence zones (Figs. 6 and 7), it is suggested that they may have been kinematically generated at the same time during the main deformation phase that affected the entire region (D_2). One possible way to explain this double vergence in an accretionary complex is to refer to the pro-wedge and retro-wedge structure that is established in wide accretionary prisms such as those described by Guillot et al. (2009), or in types C and D of subduction channels of Cloos and Shreve (1988b). In our interpretation, the lower, subducted and exhumed part (pro-wedge) would correspond to the W-vergent domains while the offscraped part (retro-wedge, in direct lateral contact with the basement) would be located in the E-vergent domain (Fig. 8). The simple shear direction would be parallel to the sections shown in Fig. 8 and opposite to both sides of the models, explaining the double vergence observed in the Maule section.

Other explanations for this double-vergence accretionary complex are certainly possible, including the activity of different tectonic phases. But the interpretation presented in this work adds to its simplicity the ability to consistently explain all the lithological, metamorphic, structural, and kinematic information and interpretations of the Maule River section. The top-to-the-E shear sense observed by Richter et al. (2007) in

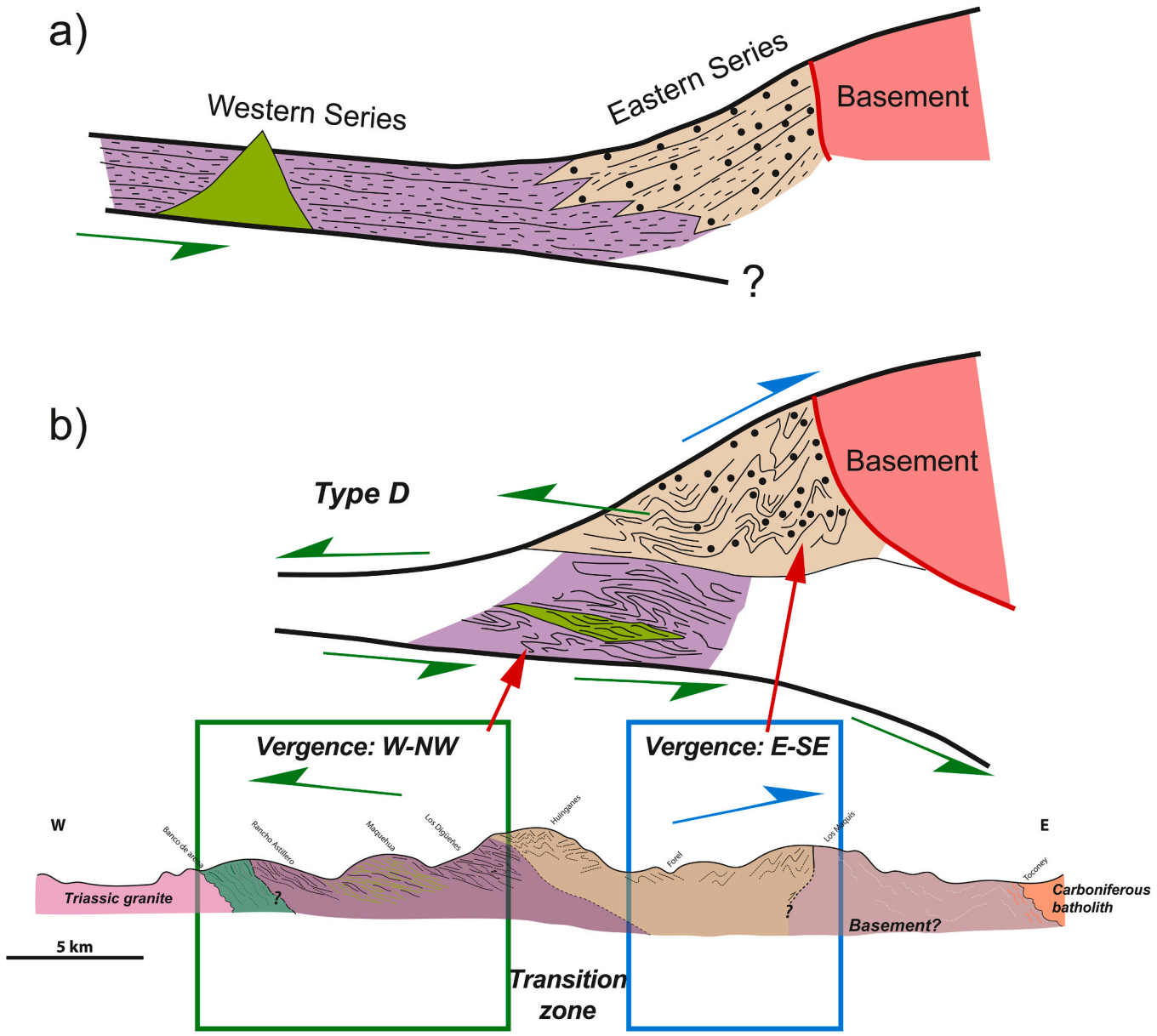

Fig. 8. a) Schematic model of the origin of the Eastern (proximal) and Western (distal) Series in an active continental margin at the end of the Paleozoic. b) Deformation of both series in a complex kinematic framework. The different structural domains of the current cross section along the Maule River (bottom cross section) and the possible location of each domain in the theoretical model are also indicated. The proposal is geometrically very similar to that presented by Richter et al. (2007, their Fig. 10b).

sectors of the Western Series can be explained by the transpression model as places where the coaxial component predominates ($W_k < 0.81$) which, according to Fig. 6, should coincide with rocks with finite-strain ellipsoids within the constriction field, situation in which it would be possible to obtain minor conjugate shear zones that are both synthetic and antithetic with respect to the major structure. The transpression model presented in this work, with shortening perpendicular to the SZBs, coincides with the tectonic interpretation given by Glodny et al. (2005) for the Western (basal accretionary complex with vertical shortening) and Eastern Series (frontally accreted units with sub-horizontal shortening).

It has been suggested for accretionary complexes in central and southern Chile that exhumation was short-lived and early in subduction history, and that exhumation rates were lower than the relative motion of the plates involved (e.g. Agard et al., 2009). Guillot et al. (2009, see references therein) have highlighted the decoupling between the subducting plate and the exhumation zone, and have listed the main mechanisms responsible for the exhumation of HP to UHP units and their incorporation into the accretionary complex. These include channel and corner flow, extensional collapse, and thrusting or buoyancy, all associated with erosion processes. Among them, they cite the "compression of a soft zone between two rigid blocks" (Thompson et al., 1997), which is similar to the extrusion process in a transpression zone. Considering that the Western Series in the Maule River section could have reached peak metamorphic conditions of 9 kbar followed by cooling and decompression below 280 °C and 8 km depth, it is appropriate to ask about its exhumation mechanism. Glodny et al. (2005) invoked the importance of erosion, while Guillot et al. (2009) alluded to a weak subduction zone, with shear zones localizing deformation and allowing the exhumation of less deformed blocks. Richter et al. (2007) proposed basal accretion of the Western Series, followed by widespread horizontal extension. Willner (2005) agrees on the process of basal accretion for the Western Series, followed by crustal thinning. Hyppolito et al. (2014a) proposed for Punta Sirena, approximately 100 km north of

the Maule River section, a first stage of subduction occurring in the subduction channel until peak metamorphism was reached, followed by an exhumation event due to forced return flow and progressive widening of the subduction channel (e.g., Gerya et al., 2002). Finally, the exhumed rocks would be incorporated into the accretionary prism at its base, from which point onward a slower exhumation episode dominated by erosion would follow. Other studies emphasize the role of underplating as the main mechanism for material transfer to the basal part of the prism, and of erosion as the dominant exhumation mechanism (Glodny et al., 2005; Menant et al., 2019, 2020). Despite the uncertainty arising from the lack of temporal constraints, in this work, we basically agree with the model of Hyppolito et al. (2014a), who insisted that the main rapid exhumation event was tectonically driven. We would add to the forced return flow process the phenomenon of extrusion associated with transpression. However, at least for the Maule River section, this extrusion cannot explain the bulk of the Western Series exhumation, since the extrusion direction formed relatively low angles ($\lesssim$30°) with respect to the shear zone strike (Fig. 6a).

5.2. *Comparison with the Chañaral mélange (Convergence style variations along the Gondwanan margin)*

The flow apophyses, defined above in section 4.2.1, can be described as directions assuming the maximum, intermediate and minimum rate of material particle displacement in a flow. In transpressional flow types such as the one used in this work, two of the flow apophyses are contained in the SZB and the third is oblique to that plane. According to Fossen and Tikoff (1998), the oblique apophysis indicates the direction of convergence between the blocks separated by the deformation zone. Consequently, the oblique apophysis has been calculated for the W- and E-vergent domains of the Maule section, taking as a starting point the values of the transpression model parameters that have shown better fits to the natural structures and fabrics. The calculated direction of the oblique apophysis (Fig. 9) can be interpreted as the direction of convergence between the blocks separated by the subduction channel. It can be observed that the results are similar for the W- and E-vergent domains. Assuming that the blocks separated by the accretionary complex correspond to two different plates, the results indicate that the Late Paleozoic direction of convergence at this plate boundary would, on average, have an orientation perpendicular to the strike of the SZB, with a possible lateral variation of up to ±24° (W-vergent domain). Considering the strike used to model the deformation zone (N033°E), the convergence direction would have a range of orientations between N099° and N147°E in the current coordinates. Given that the orientation of this convergence direction in Chañaral is N050°-060°E (Fuentes et al., 2019), the comparison between both areas leads to two conclusions (Fig. 10). Firstly, the greater perpendicularity of the vector of plate convergence in the Maule section than in the Chañaral mélange (oblique convergence, Fig. 2d) could explain the presence of rocks indicative of greater pressure in the Maule River section. This greater perpendicularity of the convergence vector in the Maule River section, with respect to the Chañaral area, would have allowed the widening of the subduction channel and a more efficient process of forced return flow. This same result may be enhanced by the arrival of oceanic roughnesses to the subduction zone (Muñoz-Montecinos et al., 2023). Secondly, the variation in the convergence direction along the Late Paleozoic margin can serve as a reference to establish the position of the rotation pole between the plates, which should be located to the N of both points (Maule and Chañaral). However, it must be taken into account that the subsequent deformation of both areas (including displacement and rotations) prevents a precise calculation of the orientation of this rotation pole (Fig. 10). It would also be necessary to confirm and complete these results by studying other contemporary accretionary prisms along the margin.

6. Concluding remarks and acknowledgment of Victor Ramos' contribution to the understanding of the Paleozoic evolution of South America

Andean studies have started to be used in the last years as proxies for older orogenic phases affecting their basement, whose evolution had classically been explained by different and independent variables. This is the case of the Paleozoic evolution of the Chilean-Argentinean Andean margin, where extensional/contractional phases and related magmatism are recently explained by the changes in the absolute displacement of South America, the roll-back velocity, maturation of the subduction system, etc, showing that phases interposed between accretional processes functioned like a subduction orogen in relation to their timing and mechanisms. In this context, Ramos and Folguera (2009)'s hypothesis of a shallow subduction regime in Early to middle Permian times (first mentioned in the thesis of A. Martínez, supervised by Prof. Victor Ramos (Martínez, 2004)), affecting a not-so-well-determined zone interposed between 27 and 37°S approximately, explains arc and deformational dynamics. This hypothesis comes from geochronological and geochemical data of different magmatic pulses between 290 and 250 Ma that abandoned the Carboniferous volcanic arc presently located between the axial and coastal Andean zones and spread through the retroarc, over the Precordillera and western Sierras Pampeanas systems, more or less

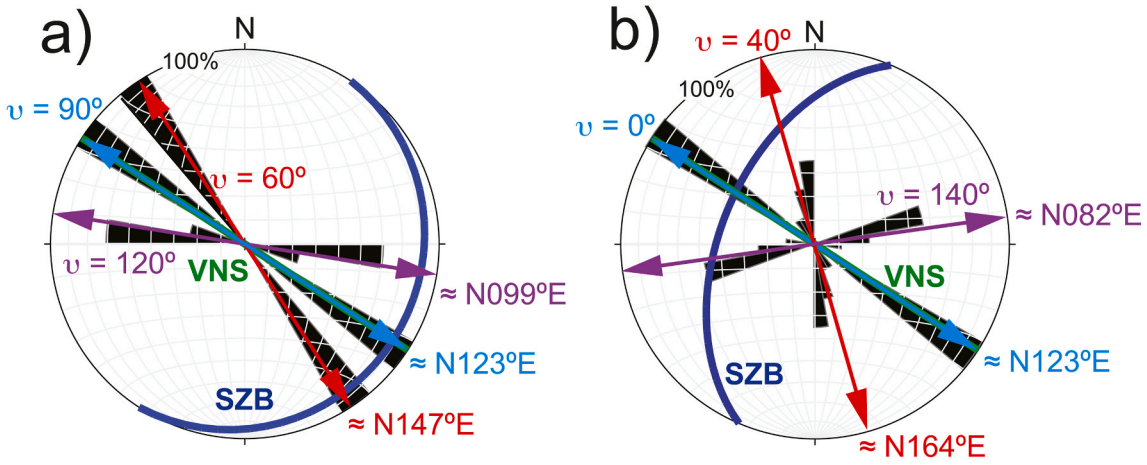

Fig. 9. - Rose diagrams showing the oblique flow apophysis (convergence direction) determined for the W-vergent domains (a) and the E-vergent domain (b), drawn on top of an equal-area, lower hemisphere projection of the SZB. In both cases, the model-estimated directions show several maxima, whose mean circular direction is indicated numerically and by double-headed arrows.

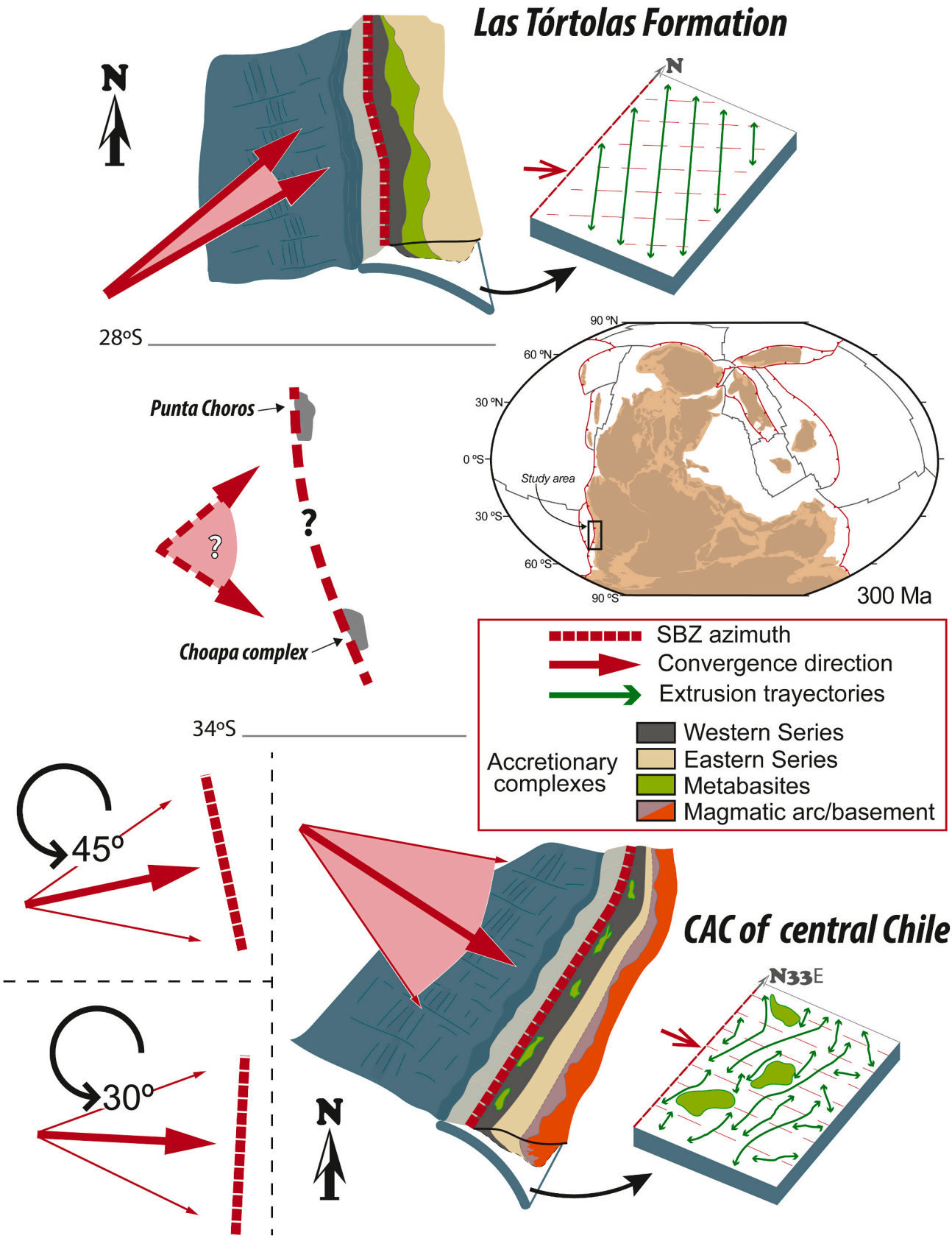

(caption on next page)

Fig. 10. - Geometric relations between the SZB (shear or subduction zone boundary) and the convergence vectors during late Paleozoic times deduced from the structural analyses of the Chañaral (Las Tórtolas Formation) and Maule (Coastal Accretionary Complex of central Chile) accretionary complexes. The figure also shows the trajectories of particles entering the subduction zone according to the results of the 3D kinematic model. Differences in the convergence style deduced from structural analysis may partially explain the differential lithological, metamorphic, and structural configuration of the Late Paleozoic accretionary complexes in northern and south-central Chile. Nevertheless, the study of other segments of the accretionary system in central and southern Chile is necessary to complete the description of the southwestern margin of Gondwana. These differences highlighted in the figure may also be accentuated by Permo-Triassic post-accretionary tectonic processes, such as tectonic erosion and exhumation, dextral block rotations (the results of counterclockwise restorations of 30 and 45° are shown in the figure), or the influence of major transcurrent structures (e.g., Lanalhue Fault zone) (Glodny et al., 2008; Kleiman and Japas, 2009; Kato and Godoy, 2015). Gondwana plate reconstruction at 300 Ma modified from Zahirovic et al. (2022).

coincidentally with the development of the late Miocene to Quaternary Chilean-Pampean flat subduction zone. Among the features that this hypothesis explains exist the Early Permian San Rafael orogenic phase, coincident with the beginning of the spreading phase of arc magmatism and the development of the syn-extensional Choi Yoi magmatic Province characterized as a within-plate volcanic association linked to the destabilization of the Permian orogen.

However, one of the weaker aspects of this proposal is the lack of correlation with deformational and magmatic phases across the entire orogen, therefore the definition of the Neopaleozoic orogenic anatomy, and the absence of a trigger as a candidate for this process that most likely should have been found inspecting the western Andean Chilean side. In this sense, the trigger for late pre-Andean (Gondwanan) processes could be inferred from the study of the accretionary complexes along the Chilean coast and the finding of obducted/offscrapped E-MORB metabasites. The peak in accretionary activity, a High Magma Addition Rate (HMAR) event in the arc, cessation of Cordilleran-type magmatism at 300–290 Ma, approximately coincide with the asynchronous arrival of oceanic reliefs or ridges to the margin between 300 and 270 Ma that could have constituted the promotion of flat subduction (e.g., Hervé et al., 1988; García San-Segundo et al., 2014; Hyppolito et al., 2014b; del Rey et al., 2016; Fuentes et al., 2018; Creixell et al., 2025). 3D structural analysis of the accretionary complexes allowed determining the complex anatomy of the accretionary prism for more than 1,000 km along the Pacific coast, from the Chañaral mélange to the Maule River section. The variation in the determined convergence direction along the Late Paleozoic margin allowed inferring the position of the rotation pole between the plates, to the N of both points (Maule and Chañaral) giving clues about the real dimensions of the allochtonous oceanic terrane.

CRediT authorship contribution statement

Juan Díaz-Alvarado: Writing – review & editing, Writing – original draft, Visualization, Validation, Supervision, Resources, Methodology, Investigation, Funding acquisition, Formal analysis, Data curation, Conceptualization. **Carlos Fernández:** Writing – review & editing, Writing – original draft, Visualization, Validation, Supervision, Software, Resources, Methodology, Investigation, Funding acquisition, Formal analysis, Data curation, Conceptualization. **Andrés Folguera:** Writing – review & editing, Writing – original draft, Validation, Supervision, Project administration, Methodology, Funding acquisition, Formal analysis. **Christian Creixell:** Writing – review & editing, Writing – original draft, Visualization, Validation, Supervision, Methodology, Investigation, Funding acquisition, Formal analysis, Data curation, Conceptualization. **Verónica Oliveros:** Writing – review & editing, Writing – original draft, Visualization, Validation, Supervision, Investigation, Funding acquisition, Conceptualization. **Juan Carlos Moral:** Writing – review & editing, Writing – original draft, Visualization, Methodology, Investigation.

Declaration of competing interest

We wish to draw the attention of the Editor to the following facts which may be considered as potential conflicts of interest and to significant financial contributions to this work.

We wish to confirm that there are no known conflicts of interest associated with this publication and there has been no significant financial support for this work that could have influenced its outcome.

We confirm that the manuscript has been read and approved by all named authors and that there are no other persons who satisfied the criteria for authorship but are not listed. We further confirm that the order of authors listed in the manuscript has been approved by all of us.

We confirm that we have given due consideration to the protection of intellectual property associated with this work and that there are no impediments to publication, including the timing of publication, with respect to intellectual property. In so doing we confirm that we have followed the regulations of our institutions concerning intellectual property.

We understand that the Corresponding Author is the sole contact for the Editorial process (including Editorial Manager and direct communications with the office). He is responsible for communicating with the other authors about progress, submissions of revisions and final approval of proofs. We confirm that we have provided a current, correct email address which is accessible by the Corresponding Author.

Acknowledgements

This research was funded by the projects: MCIN/AEI/10.13039/501100011033/. FEDER 'Una manera de hacer Europa' (REViSE-Betics-PID2020-119651RB-I00); project M3189 funded by the Rey Juan Carlos University (Research Group in Earth Dynamics and Landscape Evolution); and project IBERCRUST II/PID2021-126347NB-I00/AEI/10.13039/501100011033/FEDER,UE. We thank Monica Heilbron and Augusto Rapalini, Section Editor of Journal of South American Earth Sciences, and Jesús Muñoz-Montecinos and Cesar Witt for their detailed comments, which have significantly improved the manuscript.

Data availability

All data are included and published in the article

References

Aguirre, L., Hervé, F., Godoy, E., 1972. Distribution of metamorphic facies in Chilean outline. Krystallinikum 9, 7–19.
Allmendinger, R.W., Cardozo, N.C., Fisher, D., 2012. Structural Geology Algorithms: Vectors & Tensors. Cambridge University Press, Cambridge, UK, p. 289.
Agard, P., Yamato, P., Jolivet, L., Burov, E., 2009. Exhumation of oceanic blueschists and eclogites in subduction zones: timing and mechanisms. Earth Sci. Rev. 92, 53–79.
Bahlburg, H., 2021. A Silurian-Devonian active margin in the proto-Andes – new data on an old conundrum. Int. Geol. Rev. 64 (21), 3099–3120. https://doi.org/10.1080/00206814.2021.2012719.
Bahlburg, H., Breitkreuz, C., 1993. Differential response of a Devonian–carboniferous platform-deeper basin system to sea-level change and tectonics, N. Chilean Andes. Basin Res. 5, 21–40.
Bahlburg, H., Hervé, F., 1997. Geodynamic evolution and tectonostratigraphic terranes of NW-Argentina and N-Chile. Geol. Soc. Am. Bull. 109, 869–884.
Bahlburg, H., Vervoort, J.D., Du Frane, S.A., Bock, B., Augustsson, C., Reimann, R.C., 2009. Timing of crust formation and recycling in accretionary orogens: insights learned from the western margin of South America. Earth Sci. Rev. 97, 215–241.
Bell, C.M., 1982. The Lower Paleozoic Metasedimentary Basement of the Coastal Ranges of Chile Between 25°30′ and 27°S, vol. 17. Revista Geologica de Chile, pp. 21–29.
Bell, C.M., 1987. The origin of the upper Paleozoic Chañaral mélange of N Chile. J. Geol. Soc. Lond. 144, 599–610.

Bettelli, G., Vannucchi, P., 2003. Structural style of the offscraped Ligurian oceanic sequences of the Northern Apennines: new hypothesis concerning the development of mélange block-in-matrix fabric. J. Struct. Geol. 25, 371–388.
Charrier, R., Hervé, F., Muñoz-Gómez, M., Fanning, M., Moisan, P., Rebolledo, S., Rojas del Castillo, M., 2024. The early Carboniferous age of the Arrayán Formation in the Choapa Accretionary Complex: implications for its fossil floral content, tectonic setting and evolution of the southwestern Gondwana margin (north-central Chile). J. S. Am. Earth Sci. 148, 105161.
Cloos, M., 1982. Flow mélanges: numerical modeling and geologic constraints on their origin in the Franciscan subduction complex, California. Geol. Soc. Am. Bull. 93, 330–345.
Cloos, M., Shreve, R.L., 1988a. Subduction-channel model of prism accretion, mélange formation, sediment subduction, and subduction erosion at convergent plate margins: 1. Background and description. Pure Appl. Geophys. 128, 455–500.
Cloos, M., Shreve, R.L., 1988b. Subduction-channel model of prism accretion, mélange formation, sediment subduction, and subduction erosion at convergent plate margins: 2. Implications and discussion. Pure Appl. Geophys. 128, 501–545.
Condie, K.C., 2007. Accretionary orogens in space and time. Geol. Soc. Am. Memoirs 200, 145–158.
Creixell, C., Oliveros, V., Vásquez, P., Navarro, J., Vallejos, D., Valin, X., Godoy, E., Ducea, M.N., 2016. Geodynamics of late carboniferous early Permian forearc in north Chile (28°30′-29°30’ S). J. Geol. Soc. Lond. 173 (5), 757–772.
Creixell, C., Sepúlveda, F., Álvarez, J., Vásquez, P., Velásquez, R., 2021. The Carboniferous onset of subduction at SW Gondwana revisited: sedimentation and deformation processes along the late Paleozoic forearc of north Chile (21°–33° S). J. S. Am. Earth Sci. 107, 103149. https://doi.org/10.1016/j.jsames.2020.103149.
Creixell, C., Díaz-Alvarado, J., Álvarez, J., Rodríguez, C., Velásquez, R., Oliveros, V., 2025. Episodic magmatism and segmentation of the Gondwanan arc in Chile (21–38 °S): insights into Carboniferous to early Permian subduction processes and deformation. J. S. Am. Earth Sci. 156, 105421. https://doi.org/10.1016/j.jsames.2025.105421.
Dahlquist, J.A., Alasino, P.H., Basei, M.A.S., Morales Cámera, M.M., Macchioli Grande, M., da Costa Campos Neto, M., 2018. Petrological, geochemical, isotopic, and geochronological constraints for the Late Devonian–Early Carboniferous magmatism in SW Gondwana (27–32°S): an example of geodynamic switching. Int. J. Earth Sci. 107 (7), 2575–2603.
Dahlquist, J.A., Morales Cámera, M.M., Alasino, P.H., Pankhurst, R.J., Basei, M.A.S., Rapela, C.W., Moreno, J.A., Baldo, E.G., Galindo, C., 2021. A review of Devonian–Carboniferous magmatism in the central region of Argentina, pre-andean margin of SW Gondwana. Earth Sci. Rev. 221, 103781.
del Rey, A., Arriagada, C., Dekart, K., Martínez, F., 2016. Resolving the paradigm of the late Paleozoic-Triassic Chilean magmatism: isotopic approach. Gondwana Res. 37, 172–181.
Deckart, K., Hervé, F., Fanning, M., Ramírez, V., Calderón, M., Godoy, 2014. U–Pb geochronology and Hf–O isotopes of zircons from the Pennsylvanian Coastal Batholith, South-Central Chile. Andean Geol. 41, 49–82.
Díaz-Alvarado, J., Galaz, G., Oliveros, V., Creixell, C., Calderón, M., Horton, B.K., Folguera, A., 2019. Fragments of the late Paleozoic accretionary complex in central and northern Chile: similarities and differences as a key to decipher the complexity of the late Paleozoic to Triassic early Andean events. Andean Tectonics. Elsevier, pp. 509–530.
Díaz Azpiroz, M., Brune, S., Leever, K.A., Fernández, C., Czech, D.M., 2016. Tectonics of oblique plate boundary systems. Tectonophysics 693, 165–170.
Díaz Azpiroz, M., Fernández, C., Czeck, D.M., 2019. Are we studying deformed rocks in the right sections? Best practices in the kinematic analysis of 3D deformation zones. J. Struct. Geol. 125, 218–225. https://doi.org/10.1016/j.jsg.2018.03.005.
Escuder-Viruete, J., Baumgartner, P.O., 2014. Structural evolution and deformation kinematics of a subduction-related serpentinite-matrix mélange, Santa Elena peninsula, northwest Costa Rica. J. Struct. Geol. 66, 356–381.
Fernández, C., Díaz Azpiroz, M., 2009. Triclinic transpression zones with inclined extrusion. J. Struct. Geol. 31, 1255–1269.
Festa, A., Pini, G.A., Ogata, K., Dilek, Y., 2019. Diagnostic features and field-criteria in recognition of tectonic, sedimentary and diapiric mélanges in orogenic belts and exhumed subduction-accretion complexes. Gondwana Res. 74, 7–30.
Festa, A., Pini, G.A., Dilek, Y., Codegone, G., 2010. Mélanges and mélange-forming processes: a historical overview and new concepts. In: Dilek, Y. (Ed.), Alpine Concept in Geology International Geology Review, vol. 52, pp. 1040–1105, 10–12.
Festa, A., Dilek, Y., Pini, G.A., Codegone, G., Ogata, K., 2012. Mechanisms and processes of stratal disruption and mixing in the development of mélanges and broken formations: redefining and classifying mélanges. Tectonophysics 568, 7–24.
Fossen, H., 2016. Structural Geology, second ed. Cambridge Univ. Press, Cambridge, UK, p. 524.
Fossen, H., Cavalcante, G.C.G., 2017. Shear zones – a review. Earth-Sciences Reviews 171, 434–455.
Fossen, H., Tikoff, B., 1998. Extended models of transpression and transtension, and application to tectonic settings. In: Holdsworth, R.E., Strachan, R.A., Dewey, J.F. (Eds.), Continental Transpressional and Transtensional Tectonics, vol. 135. Geological Society, London, Special Publications, pp. 15–33.
Fuentes, P., Díaz-Alvarado, J., Fernández, C., Díaz Azpiroz, M., Rodríguez, N., 2016. Structural analysis and shape-preferred orientation determination of the mélange facies in the Chañaral mélange, Las Tórtolas Formation, coastal cordillera, northern Chile. J. S. Am. Earth Sci. 67, 40–56.
Fuentes, P., Díaz-Alvarado, J., Rodríguez, N., Fernandez, C., Breitkreuz, C., Contreras, A., 2018. Geochemistry, petrogenesis and tectonic significance of the volcanic rocks of the Las Tortolas formation, coastal cordillera, northern Chile. J. S. Am. Earth Sci. 87, 66–86. https://doi.org/10.1016/j.jsames.2017.11.006.
Fuentes, P., Fernández, C., Díaz-Alvarado, J., Díaz Azpiroz, M., 2019. Using 3D kinematic models in subduction channels. The case of the Chañaral tectonic mélange, Coastal Cordillera, northern Chile. Gondwana Res. 74, 251–270.
Gana, P., Hervé, F., 1983. Geología del basamento cristalino de la Cordillera de la Costa entre los ríos Mataquito y Maule, VII Región. Rev. Geol. Chile 19, 37–56.
Gana, P., Tosdal, R., 1996. Geocronología U-Pb y K-Ar en intrusivos del Paleozoico y Mesozoico de la Cordillera de la Costa, Región de Valparaíso, Chile. Rev. Geol. Chile 23 (2), 151–164.
García-Sansegundo, J., Farias, P., Heredia, N., Gallastegui, G., Charrier, R., Rubio Ordóñez, A., Cuesta, A., 2014. Structure of the Andean Palaeozoic basement in the Chilean coast at 31°30’ S: geodynamic evolution of a subduction margin. J. Iber. Geol. 40 (2), 293–308.
García-Sansegundo, J., Farias, P., Gallastegui, G., Heredia, N., Cuesta, A., Rubio-Ordóñez, A., Martín-González, F., Santos-Martínez, J., Palape, C., García-Moreno, O., 2023. Paleozoic gondwanan structure along the maule river valley between toconey and constitución (35.4°S, chilean pacific coast). J. S. Am. Earth Sci. 123, 104246. https://doi.org/10.1016/j.jsames.2023.104246.
Gerya, T.V., Stöckhert, B., Perchuk, A.L., 2002. Exhumation of high-pressure metamorphic rocks in a subduction channel: a numerical simulation. Tectonics 21, 1056. https://doi.org/10.1029/2002TC001406.
Glodny, J., Lohrmann, J., Echtler, H., Gräfe, K., Seifert, W., Collao, S., Figueroa, O., 2005. Internal dynamics of a paleoaccretionary wedge: insights from combined isotope tectonochronology and sandbox modelling of the South Central Chilean forearc. Earth Planet Sci. Lett. 231, 23–39.
Glodny, J., Echtler, H., Collao, S., Ardiles, M., Burón, P., Figueroa, O., 2008. Differential late Paleozoic active margin evolution in south-central Chile (37°S-40°S)—The Lanalhue fault zone. J. S. Am. Earth Sci. 26, 397–411.
Godoy, E., Loske, W., 1988. Tectonismo sinplutónico de dioritas jurásicas al sur de Valparaíso: datos U–Pb sobre la Fase Quintay. Rev. Geol. Chile 15, 119–127.
Grigull, S., Krohe, A., Moos, C., Wassmann, S., Stöckhert, B., 2012. “Order from chaos”: a field-based estimate on bulk rheology of tectonic mélanges formed in subduction zones. Tectonophysics 568, 86–101.
Guillot, S., Hattori, K., Agard, P., Schwartz, S., Vidal, O., 2009. Exhumation processes in oceanic and continental subduction contexts: a review. In: S. Lallemand, S., Funiciello, F. (Eds.), Subduction Zone Geodynamics. Springer-Verlag, pp. 175–205.
Heredia, N., García-Sansegundo, J., Gallastegui, G., Farias, P., Giacosa, R., Alonso, J., Busquets, P., Charrier, R., Clariana, P., Colombo, F., Cuesta, Gallastegui A.J., Giambiagi, L., González-Menéndez, L., Limarino, C.O., Martín-González, F., Méndez-Bedia, I., Pedreira, D., Quintana, L., Rodríguez-Fernández, L.R., Rubio-Ordóñez, A., Seggiaro, R., Serra-Varela, S., Spalletti, L., Cardó, R., Ramos, V., 2016. Evolución Geodinámica de los Andes argentino-chilenos y la Península Antártica durante el Neoproterozoico tardío y el Paleozoico. Trab. Geol. 36, 237–278. Universidad de Oviedo.
Heredia, N., García-Sansegundo, J., Gallastegui, G., Farias, P., Giacosa, R.E., Giambiagi, L.B., Busquets, P., Colombo, F., Charrier, R., Cuesta, A., Rubio-Ordóñez, A., Ramos, V.A., 2017. Review of the geodynamic evolution of the SW margin of Gondwana preserved in the Central Andes of Argentina and Chile (28°-38° S latitude). J. S. Am. Earth Sci. 87, 87–94. https://doi.org/10.1016/j.jsames.2017.11.019.
Hervé, F., 1977. Petrology of the crystalline basement of the Nahuelbuta mountains, south central Chile. In: Ishikawa, T., et al. (Eds.), Comparative Studies on the Geology of the CircumPacific Orogenic Belt in Japan and Chile. Japanese Society for the Promotion of Sciences, pp. 1–51.
Hervé, F., 1988. Late Paleozoic subduction and accretion in Southern Chile. Episodes 11, 183–188.
Hervé, F., Munizaga, F., Parada, M.A., Brook, M., Pankhurst, R.J., Snelling, N.J., Drake, R., 1988. Granitoids of the Coast Range of central Chile: geochronology and geologic setting. J. S. Am. Earth Sci. 1 (2), 185–194. https://doi.org/10.1016/0895-9811(88)90036-3.
Hervé, F., Calderón, M., Fanning, M., Pankhurst, R., Godoy, E., 2013. Provenance variations in the late Paleozoic accretionary complex of central Chile as indicated by detrital zircons. Gondwana Res. 23, 1122–1135.
Hervé, F., Calderón, M., Fanning, C.M., Pankhurst, R.J., Fuentes, F., Rapela, C.W., Marambio, C., 2016. Devonian magmatism in the accretionary complex of southern Chile. J. Geol. Soc. 173, 587–602.
Hervé, F., Calderón, M., Fanning, C.M., Pankhurst, R.J., Rapela, C.W., Quezada, P., 2018. The country rocks of Devonian magmatism in the North Patagonian Massif and Chaitenia. Andean Geol. 45 (3), 301–317. https://doi.org/10.5027/andgeoV45n3-3117.
Hyppolito, T., Garcia-Casco, A., Juliani, C., Meira, V.T., Hall, C., 2014a. Late Paleozoic onset of subduction and exhumation at the western margin of Gondwana (Chilenia Terrane): counterclockwise P-T paths and timing of metamorphism of deep-seated garnet-mica schist and amphibolite of Punta Sirena, coastal Accretionary complex. Lithos 216–217, 409–434.
Hyppolito, T., Juliani, C., García-Casco, A., Meira, V.T., Bustamante, A., Hervé, F., 2014b. The nature of the Paleozoic oceanic basin at the southwestern margin of Gondwana and implications for the origin of the Chilenia terrane (Pichilemu region, central Chile). Int. Geol. Rev. 56 (9), 1097–1121.
Hyppolito, T., Juliani, C., Garcia-Casco, A., Meira, V., Bustamante, A., Hall, C., 2015. LP/HT metamorphism as a temporal marker of change of deformation style within the late Palaeozoic accretionary wedge of central Chile. J. Metamorph. Geol. 33 (9), 1003–1024.
Jorquera, R., Domagala, J., Villa, V., Astudillo, N., 2023. Geología del área Pichibelco-Cauquenes, región del Maule. Servicio Nacional de Geología y Minería, Carta Geológica de Chile, Serie Geología Básica 214, 151, 1 mapa escala 1:100.000. Santiago.

Kato, T.T., Godoy, E., 2015. Middle to late Triassic mélange exhumation along a pre-andean transpressional fault system: coastal Chile (26°-42° S). Int. Geol. Rev. 57 (5–8), 606–628.
Kimura, G., Kitamura, Y., Hashimoto, Y., Yamaguchi, A., Shibata, T., Ujiie, K., Okamoto, S., 2007. Transition of accretionary wedge structures around the up-dip limit of the seismogenic subduction zone. Earth Planet Sci. Lett. 255, 471–484.
Kleiman, L.E., Japas, M.S., 2009. The Choiyoi volcanic province at 34°S-36°S (San Rafael, Mendoza, Argentina): implications for the late Paleozoic evolution of the southwestern margin of Gondwana. Tectonophysics 473, 283–299. https://doi.org/10.1016/j.tecto.2009.02.046.
Limarino, C.O., Heredia, N., Spalletti, L., Busquets, P., Colombo, F., Méndez-Bedia, I., Cardó, R., Césari, S., 2023. Stratigraphy and tectosedimentary evolution of the late Paleozoic Ancestral Andes between 33◦ and 25◦ SL. J. S. Am. Earth Sci. 121, 104116.
Lin, S., Jiang, D., Williams, P.F., 1998. Transpression (or transtension) zones of triclinic symmetry: natural example and theoretical modelling. In: Holdsworth, R.E., Strachan, R.A., Dewey, J.F. (Eds.), Continental Transpressional and Transtensional Tectonics, vol. 135. Geological Society, London, Special Publications, pp. 41–57.
Marioth, R., 2001. Characterisierung Und Quantifizierung Thermischer Und Diagenetischer Prozesse Im Karbonischen Akkretionsprisma in Nordchile. Univ. Heidelberg, Germany, p. 144. PhD Thesis.
Marioth, R., Bahlburg, H., 2003. Characterisation and quantification of thermal and diagenetic processes in the carboniferous accretionary prism (Chañaral Mélange) in northern Chile. In: IGCP 436 Final Symposium: Evolution of the Gondwana Margin, X Congreso Geológico Chileno. Actas.
Martínez, A.N., 2004. Secuencias volcánicas permo-triásicas de los cordones del Portillo y del Plata, Cordillera frontal, Mendoza : su interpretación tectónica. Tesis Doctoral. Universidad de Buenos Aires. Facultad de Ciencias Exactas y Naturales 279.
Menant, A., Angiboust, S., Gerya, T., 2019. Stress-driven fluid flow controls long-term megathrust strength and deep accretionary dynamics. Sci. Rep. 9 (1), 1–11. https://doi.org/10.1038/s41598-019-46191-y.
Menant, A., Angiboust, S., Gerya, T., Lacassin, R., Simoes, M., Grandin, R., 2020. Transient stripping of subducting slabs controls periodic forearc uplift. Nat. Commun. 11 (1), 1–10. https://doi.org/10.1038/s41467-020-15580-7.
Miller, H., 1970. Vergleichende Studien an prämesozoischen Gesteine Chile unter besonderen Berucksichtigung ihrer Kleintektonik. Geotekt. Forsch. 36, 1–64.
Munoz-Montecinos, J., Angiboust, S., Cambeses, A., García-Casco, A., 2020. Multiple veining in a paleo–accretionary wedge: the metamorphic rock record of prograde dehydration and transient high pore-fluid pressures along the subduction interface (Western Series, central Chile). Geosphere 16 (3), 765–786. https://doi.org/10.1130/GES02227.1.
Munoz-Montecinos, J., Cambeses, A., Angiboust, S., 2023. Accretion and subduction mass transfer processes: Zircon SHRIMP and geochemical insights from the Carboniferous Western Series, Central Chile. Int. Geol. Rev. 66, 54–80. https://doi.org/10.1080/00206814.2023.2185822.
Niwa, M., 2006. The structure and kinematics of an imbricate stack of oceanic rocks in the Jurassic accretionary complex of Central Japan: an oblique subduction model. J. Struct. Geol. 28 (9), 1670–1684.
Ohsumi, T., Ogawa, Y., 2008. Vein structures, like ripple marks, are formed by shortwavelength shear waves. J. Struct. Geol. 30 (6), 719–724.
Otamendi, J.E., Cristofolini, Morosini, Armasa, P., Tibaldi, A.M., Camilletti, G.C., 2020. The geodynamic history of the famatinian arc, Argentina: a record of exposed geology over the type section (latitudes 27°- 33° south). J. S. Am. Earth Sci. 100, 102558.
Passchier, C.W., 1997. The fabric attractor. J. Struct. Geol. 19, 113–127.
Philippon, M., Corti, G., 2016. Obliquity along plate boundaries. Tectonophysics 693, 171–182.
Plunder, A., Thieulot, C., van Hinsbergen, D.J.J., 2018. The effect of obliquity on temperature in subduction zones: insights from 3-D numerical modeling. Solid Earth 9, 759–776.
Ramos, V.A., Folguera, A., 2009. Andean flat subduction through time. In: Murphy, B., Keppie, J., Hynes, A. (Eds.), Ancient Orogens and Modern Analogues, vol 327. Geological Society of London, Special Publication, pp. 31–54. Geological Society, London, Special Publications.
Ramsay, J.G., Huber, M.I., 1983. The Techniques of Modern Structural Geology. Volume 1: Strain Analysis. Academic Press, London, p. 307.
Raymond, L.A., 1984. Classification of mélanges. In: Raymond, L.A. (Ed.), Mélanges: Their Nature, Origin and Significance, vol. 198. Geological Society of America Special Papers, Boulder, Colorado, pp. 7–20.
Richter, P.P., Ring, U., Willner, A.P., Leiss, B., 2007. Structural contacts in subduction complexes and their tectonic significance: the late Palaeozoic coastal accretionary wedge of central Chile. J. Geol. Soc. 164, 203–214. London.
Shi, Y., Yu, J.H., Santosh, M., 2013. Tectonic evolution of the Qinling orogenic belt, Central China: new evidence from geochemical, zircon UePb geochronology and Hf isotopes. Precambr. Res. 231, 19–60.
Shreve, R.L., Cloos, M., 1986. Dynamics of sediment subduction, mélange formation, and prism accretion. J. Geophys. Res. 91, 10229–10245.
Steenken, A., Rabbia, O., Fazzito, S., Chipana, E., Pino, E., Hernández, L., Quinzio, L.A., González, A., Bonilla, R., 2022. Structural characterization by anisotropy of magmatic fabrics and microstructures of the Nahuelbuta batholith and its emplacement within the metamorphic complex of the eastern series, south-Central Chile. N. Jb. Geol. Paläont. Abh. 305/1, 39–74.
Taira, A., Byrne, T., Ashi, J., 1992. Photographic Atlas of an Accretionary Prism: Geological Structures of the Shimanto Belt. Springer-Verlag and University of Tokyo Press, Japan: Tokyo, p. 124.
Thompson, A., Schulmann, K., Jezek, J., 1997. Extrusion tectonics and elevation of lower crustal metamorphic rocks on convergent orogens. Geology 25, 491–494.
Truesdell, C.A., 1953. Two measures of vorticity. Journal of Rational Mechanical Analysis 2, 173–217.
Ulricksen, C., 1979. Regional Geology, Geochronology and Metallogeny of the Coastal Cordillera of Chile Between 25°30′ and 26°00′ South. Dalhousie University, Canada. PhD Thesis.
Velásquez, R., Merino, R., Creixell, C., 2024. New U-Pb zircons and Ar-Ar micas ages or the Southern Coastal Batholith of Central Chile in Maule and Biobío regions, Chile. In: *Book of Abstracts of the XIII South American Symposium on Isotope Geology*, 2024, Búzios. Anais Eletrônicos. Campinas, Galoá, 2024.
Webb, L., Klepeis, K., 2019. $^{40}Ar/^{39}Ar$ constraints on the tectonic evolution of the late Paleozoic and early Mesozoic accretionary complex of coastal central Chile. In: Horton, B., Folguera, A. (Eds.), Andean Tectonics. Elsevier, pp. 531–553. https://doi.org/10.1016/B978-0-12-816009-1.00020-4.
Weinberg, R.F., Becchio, R., Farias, P., Suzaño, N., Sola, A., 2018. Early Paleozoic accretionary orogenies in NW Argentina: growth of West Gondwana. Earth Sciences Review 187, 219–247. https://doi.org/10.1016/j.earscirev.2018.10.001.
Williams, P.F., 1976. Relationships between axial-plane foliations and strain. Tectonophysics 30, 181–196.
Willner, A.P., 2005. Pressure-temperature evolution of a Late Paleozoic paired metamorphic belt in north-central Chile (34–35 30'S). J. Petrol. 46, 1805–1833.
Willner, A.P., Thomson, S.N., Kröner, A., Wartho, J.A., Wijbrans, J.R., Hervé, F., 2005. Time markers for the evolution and exhumation history of a late Paleozoic paired metamorphic belt in north-central Chile (34°-35° 30' S). J. Petrol. 46, 1835–1855.
Willner, A.P., Massonne, H.-J., Ring, U., Sudo, M., Thomson, S.N., 2012. P-T evolution and timing of a late Paleozoic fore-arc system and its heterogeneous Mesozoic overprint in north-central Chile (latitudes 31- 32°S). Geol. Mag. 149, 177–207.
Xypolias, P., 2010. Vorticity analysis in shear zones: a review of methods and applications. J. Struct. Geol. 32, 2072–2092.
Zahirovic, S., Eleish, A., Doss, S., Pall, J., Cannon, J., Pistone, M., 2022. Subduction and carbonate platform interactions. Geoscience Data Journal 9 (2), 371–383. https://doi.org/10.1002/gdj3.146.